The Formation of the North Qilian Shan through Time: Clues from Detrital Zircon Fission-Track Data from Modern River Sediments

Xu Lin, Marc Jolivet, Jing Liu-Zeng, Feng Cheng, Zhonghai Wu, Yuntao Tian, Lingling Li, Jixin Chen

geosciences

MDPI

Article

The Formation of the North Qilian Shan through Time: Clues from Detrital Zircon Fission-Track Data from Modern River Sediments

Xu Lin [1,2,*], Marc Jolivet [3,*], Jing Liu-Zeng [4], Feng Cheng [5], Zhonghai Wu [6], Yuntao Tian [7], Lingling Li [1] and Jixin Chen [1]

1 College of Civil Engineering and Architecture, China Three Gorges University, Yichang 443002, China; lilingling@ctgu.edu.cn (L.L.); chenjixin@ctgu.edu.cn (J.C.)
2 Collaborative Innovation Center for Geo-Hazards and Eco-Environment in Three Gorges Area, China Three Gorges University, Yichang 443002, China
3 Laboratoire G'eosciences Rennes, CNRS-UMR6118, Universit'e Rennes 1, Observatoire des Sciences de l'Univers, 35042 Rennes, France
4 School of Earth System Science, Tianjin University, Tianjin 300072, China; liu_zeng@tju.edu.cn
5 School of Earth and Space Sciences, Peking University, Beijing 100871, China; chengfeng@pku.edu.cn
6 Institute of Geological Mechanics, Chinese Academy of Geological Science, Beijing 100081, China; wuzhonghai8848@foxmail.com
7 Guangdong Provincial Key Laboratory of Geodynamics and Geohazards, School of Earth Sciences and Engineering, Sun Yat-sen University, Guangzhou 510275, China; tianyuntao@mail.sysu.edu.cn
* Correspondence: linxu@ctgu.edu.cn (X.L.); marc.jolivet@univ-rennes1.fr (M.J.)

Abstract: Understanding the formation of the North Qilian Shan in the NE Tibetan Plateau provides insights into the growth mechanisms of the northern region of the plateau across time. Detrital zircon fission-track (ZFT) analyses of river sediments can provide a comprehensive understanding of the exhumation history during prolonged orogenesis. Here, we applied the detrital thermochronology approach to the Qilian Shan orogenic belt. This work presents the first single-grain detrital ZFT data from river-bed sediments of the upper Hei River catchment in North Qilian Shan. The single ZFT ages are widely distributed between about 1200 Ma and about 40 Ma. These data record the protracted history of the Qilian Shan region from the Neoproterozoic evolution of Rodinia and late Paleozoic amalgamation of Central Asia to the accretion of the Gondwanian blocks during the Meso-Cenozoic era. Strong post-magmatic cooling events occurred in North Qilian Shan at 1200~1000 Ma, corresponding to the assembly of the Rodinia supercontinent. The age population at 800 Ma documents the oceanic spreading in the late Neoproterozoic dismantling of Rodinia. ZFT ages ranging from about 750 Ma to 550 Ma (with age peaks at 723 Ma and 588 Ma) are consistent with the timing of the opening and spreading of the Qilian Ocean. The age peaks at 523 Ma and 450 Ma mark the progressive closure of that ocean ending with the collision of the Qilian block with the Alxa block—North China craton in the Devonian. The Qilian Ocean finally closed in Late Devonian (age peak at 375 Ma). In the late Paleozoic (275 Ma), the subduction of the Paleotethys Ocean led to extensive magmatic activity in the North Qilian Shan. During the Lower Cretaceous (145 Ma), the accretion of the Lhasa block to the south (and potentially the closure of the Mongol-Okhotsk Ocean to the northeast) triggered a renewed tectonic activity in the Qilian Shan. Finally, a poorly defined early Eocene exhumation event (50 Ma) suggests that the NE Tibetan Plateau started to deform nearly synchronously with the onset of the India-Asia collision. This study demonstrates the usefulness of combining modern-river detrital thermo-/geochronological ages and bedrock geochronological ages to understand large-scale orogenic evolution processes.

Keywords: North Qilian Shan; Hei River; zircon fission track; LA-ICP-MS

Citation: Lin, X.; Jolivet, M.; Liu-Zeng, J.; Cheng, F.; Wu, Z.; Tian, Y.; Li, L.; Chen, J. The Formation of the North Qilian Shan through Time: Clues from Detrital Zircon Fission-Track Data from Modern River Sediments. *Geosciences* **2022**, *12*, 166. https://doi.org/10.3390/geosciences12040166

Academic Editors: Olivier Lacombe and Jesus Martinez-Frias

Received: 26 February 2022
Accepted: 4 April 2022
Published: 7 April 2022

1. Introduction

The Qilian Shan is a NW-SE trending orogenic belt forming the northeastern margin of the Tibetan Plateau [1–8] (Figure 1A). The topography and exhumation pattern of the range provide a complete record of the timing and style of exhumation of the NE Tibetan Plateau during the Cenozoic orogeny [9–16] (Figure 1B,C). The tectonic evolution of the Qilian Shan is still highly debated between two main models: (1) the whole uplift of the Qilian Shan coincided with the collision time of India and Eurasia in the early Cenozoic [1]; or (2) the Qilian Shan gradually uplifted from south to north and became a part of the northeastern margin of the Tibetan Plateau in the Late Miocene to the Pliocene [17]. The range also preserved fragments of the paleogeography and thermal structure prevailing prior to the India-Asia collision [2,18–22]. However, the characteristics of that pre-Cenozoic landscape are also debated, especially the potential occurrence of a Mesozoic plateau [23–27]. Therefore, while the Qilian Shan represents a unique object to assess and quantify the geodynamic processes that controlled the formation and extent of the Tibetan Plateau, many uncertainties still remain that require further data [2,28–32].

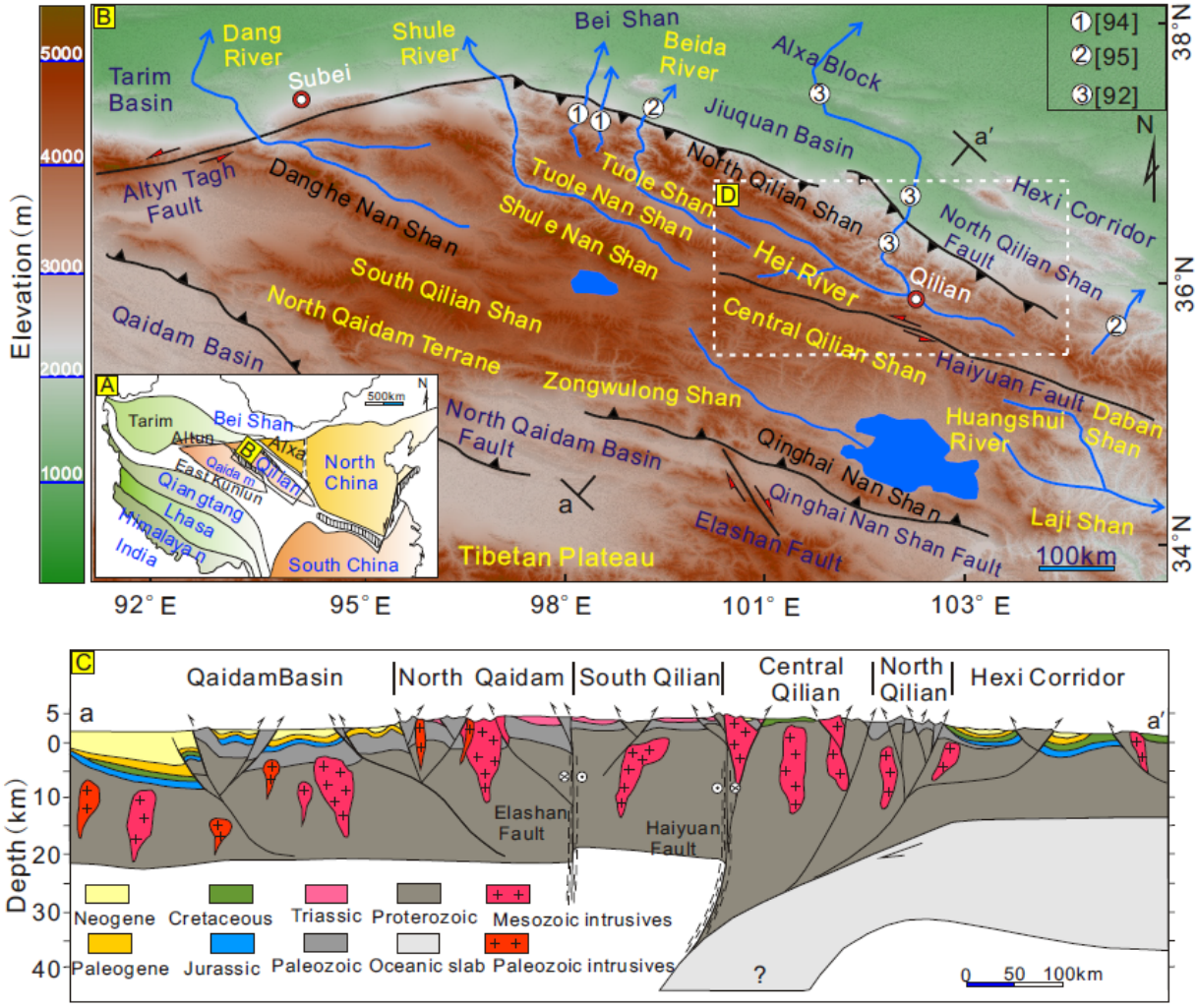

Figure 1. *Cont.*

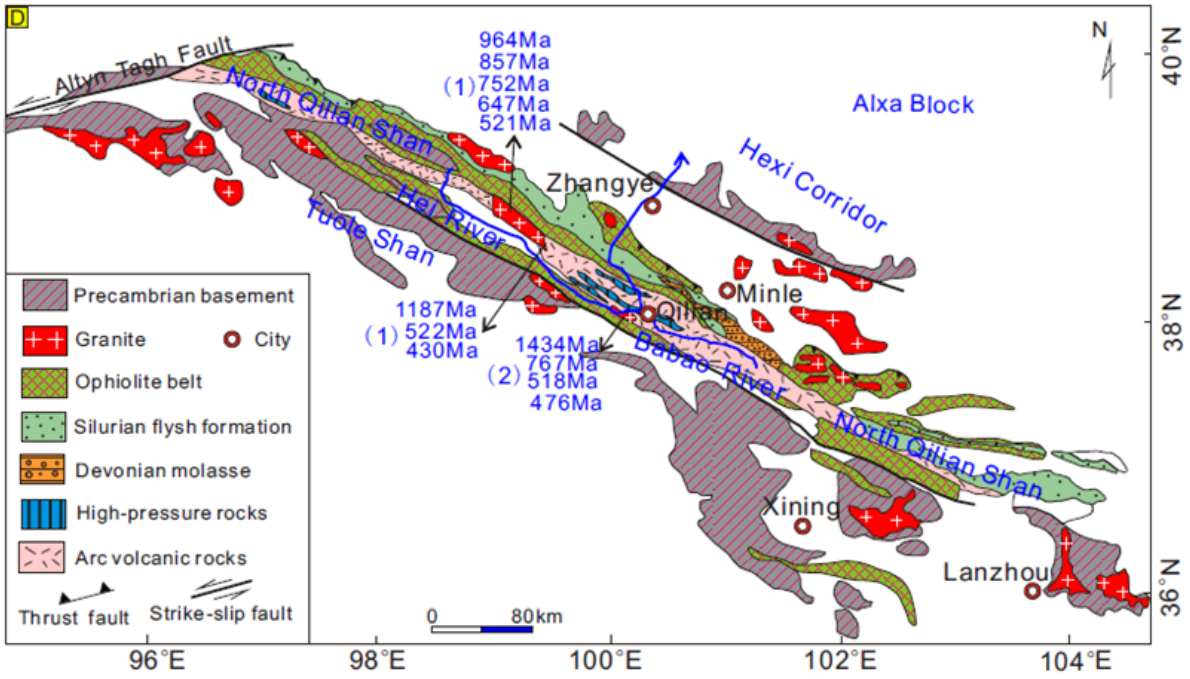

Figure 1. (**A**) Main structural blocks forming the Tibetan Plateau and its surrounding regions Modified from [33]); (**B**) map showing the major rivers draining the Qilian Shan and adjacent regions. The numbers in white circles refer to published fluvial detrital zircon analysis studies; (**C**) schematic geological cross-section of the a–a′ trace in Figure 1B (Modified from [16]); (**D**) simplified geological map and granite zircon U-Pb sampling locations along the upper reaches of the Hei River. This map is re-drawn from [6]; Zircon U-Pb ages are from (1) [6,34,35]; (2) [36,37]).

The zircon U-Pb geochronological system, with closure temperatures of 900–700 °C is highly resistant to thermal overprinting and therefore, in the absence of major metamorphic fluid circulation [38], largely preserves magmatic or high-grade metamorphic ages [39–41]. U-Pb geochronology, applied to basement rocks and associated to structural and petrographic studies has been widely used to constrain the Paleozoic early formation of the North Qilian Shan, a sub-range corresponding to the frontal part of the Qilian Shan. This early evolution proved to be geodynamically complex, implying major exhumation phases driven by crustal growth, accretion, and collision events [32,42,43]. In contrast, the effects of the Cenozoic phase appear more limited, with exhumation being restricted to the upper crust. In that context, low temperature dating methods such as apatite fission tracks (AFT) and (U-Th)/He (AHe) (thermal sensitivity ranges of the systems are 120–60 °C and 80–40 °C, respectively) have proven to be essential to investigate the ongoing orogeny [2,9,22,44–46]. Nonetheless, when considering the various approaches used to constrain the timing of onset of exhumation phases in the well-studied North Qilian Shan sub-range, little consensus has been reached: ~60–50 Ma [13,22,47], 40–30 Ma [2,10,48], 20–10 Ma [49–52], and ~7–5 Ma [53–55]. The discrepancies between those results are linked to the peculiar thermal state of the range that partly preserved the Mesozoic thermal pattern unevenly overprinted by the Cenozoic one.

When studying the tectonic evolution of a mountain range, bedrock multi-methods thermochronological dating has the advantage of recording the cooling of rocks at a specific location over a wide range of temperatures. However, access to exposed bedrock can be limited due, for example, to thick vegetation, ice cover, or steep slopes, preventing an exhaustive coverage of the studied range. On the contrary, thermochronological dating of detrital minerals in sedimentary basins adjacent to the orogen provide an integrated, large-scale record of the exhumation history of the range [56–59]. Erosional material produced over the whole area of a given drainage system is ultimately collected into the river network.

Detrital thermochronology of modern river sediments thus represents a unique opportunity to assess the large-scale exhumation history of an orogen [30,60–67] (Figure 2).

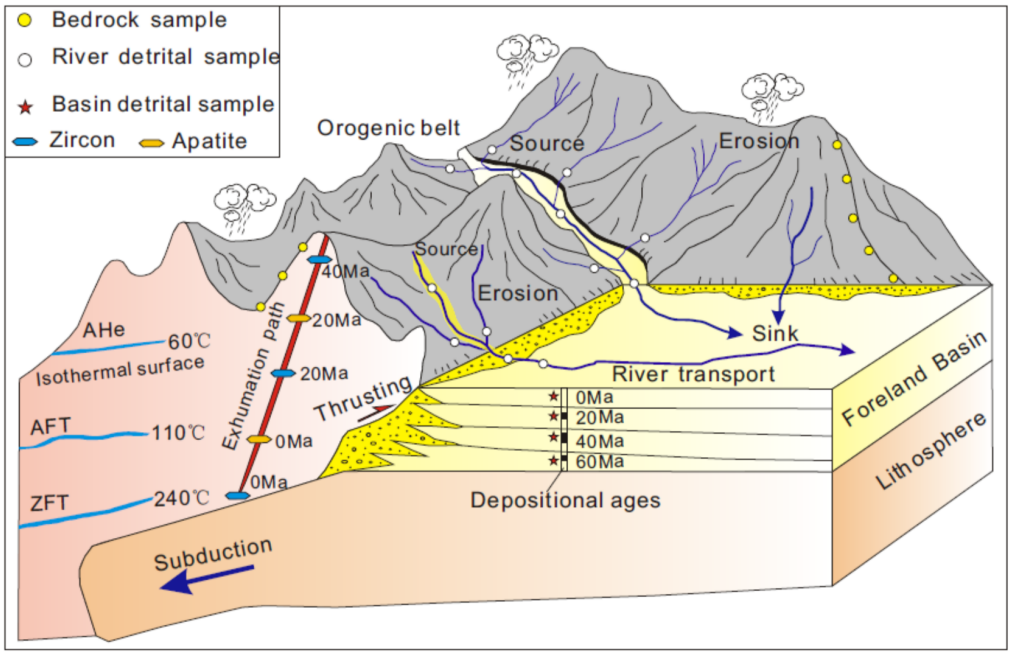

Figure 2. Cartoon showing the source-to-sink relationship between bedrock erosion and foreland deposition. The exhumation path can be restored by either bedrock low-temperature thermochronology data (AHe, AFT, and ZFT) from the orogen or detrital data from the foreland basin and river sediments.

Zircon fission-track (ZFT) closure temperature is about 240 ± 20 °C [68,69], allowing the investigation of deeper (and generally older) exhumation events than the lower temperature AFT and AHe methods [2,70,71]. Applied to the North Qilian Shan, the method should thus provide access to the Mesozoic thermal pattern allowing deconvolution of the two signals in areas where the lower temperature signal has been overprinted by the Cenozoic cooling phase. In this work we report the first fission-track analysis results on detrital zircons obtained from modern sands of the Hei River that flows from the North Qilian Shan down to the Hexi corridor (Figure 1). We combine our detrital ZFT results with published detrital and bedrock thermochronological data, zircon U-Pb ages, and stratigraphic studies to investigate the long-term exhumation history of the North Qilian Shan and improve our understanding of the long-term evolution of the NE Tibetan Plateau region.

2. Geological Setting

2.1. Qilian Shan

The Qilian Shan separates the Qaidam Basin from the North China Craton (Figure 1B) and reach peak elevations of ~5500 m for a mean surface elevation of ~4000 m. The range is composed of a series of NW-SE-trending mountains, including in its northern part, the North Qaidam Terrane, the South Qilian Shan, the Danghe Nan Shan, the Shule Nan Shan, the Tuole Shan and the North Qilian Shan. These sub-ranges are separated by several major active thrust and strike-slip faults, namely the North Qilian Fault, the Haiyuan Fault and the North Qaidam Basin Fault [53,72,73].

The North Qilian Shan basement is formed by a typical oceanic suture zone facies association [6,32,33]. It includes Neoproterozoic to early Paleozoic ophiolite sequences, ultra-high pressure metamorphic belts, island-arc volcanic rocks and granitoids (Figure 1D). The North Qilian Shan preserves evidence for the initial assembly of the Rodinia supercontinent (1100–900 Ma), the extension and rifting events (900–750 Ma) that finally led to continental breakup (750–600 Ma) [73,74] (Figure 3A). Following the break-up of the

Rodinia supercontinent, the Qilian Ocean opened, spreading during 750–520 Ma [6,75] (Figure 3B). Continental plates movements led to the final closure of the Qilian oceanic basin in Ordovician-Silurian times following the subduction of the North Qilian paleo-ocean under the Alxa block (the present-day western part of the North China block) [1,6,33,73,74] (Figure 3C). The associated sedimentary sequence is composed of Silurian flysch deposits and Devonian molasse (Xu et al., 2010; Zuza et al., 2018). Subsequently, the subduction of the Paleo-Tethys Ocean during the late Paleozoic triggered several magmatic and metamorphic events accompanied by varying degrees of uplift and exhumation within the North Qilian Shan region [40,42,76,77] (Figure 3D).

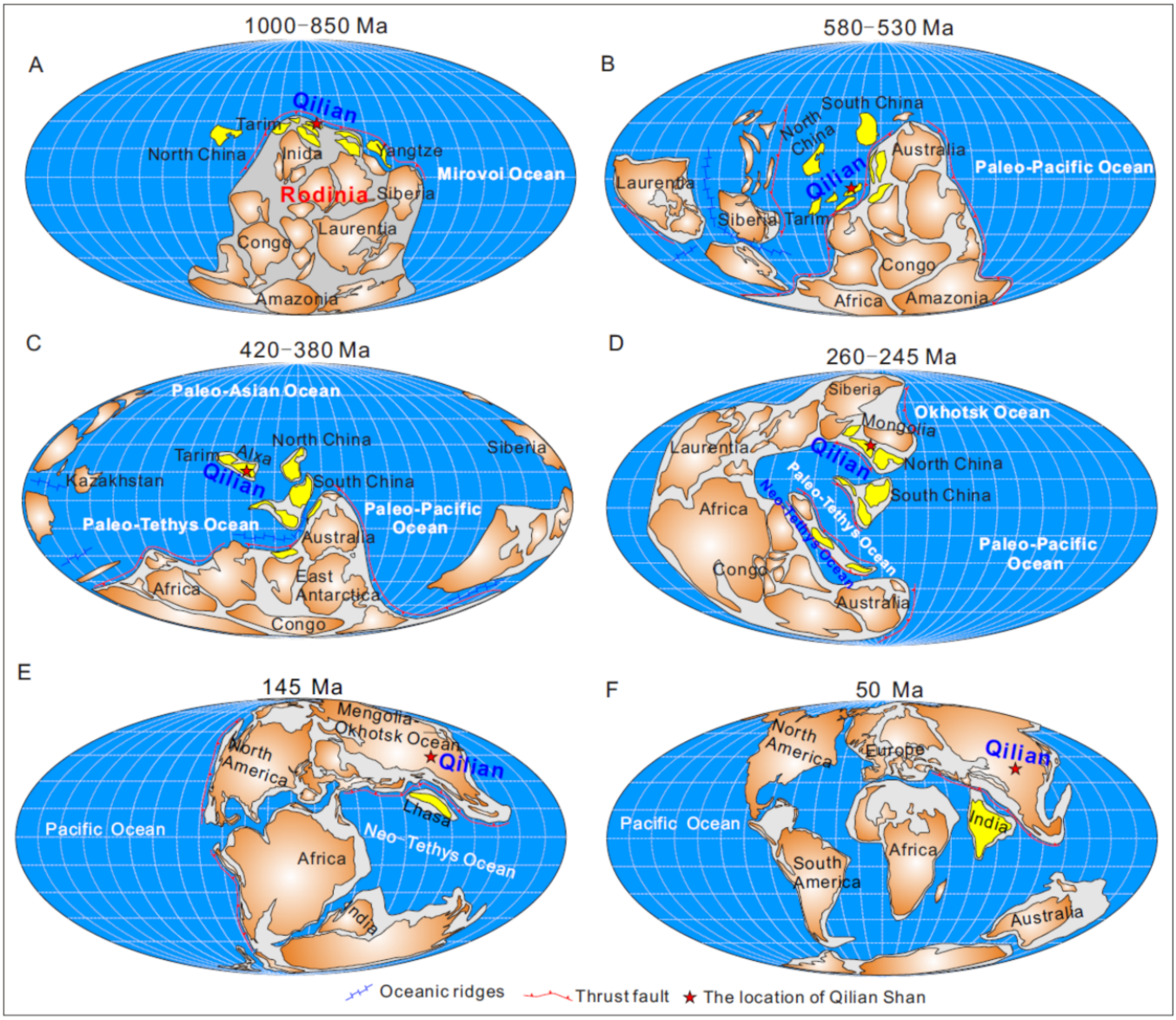

Figure 3. Meso-Neoproterozoic and Cenozoic paleogeographic maps (Modifed from [73,78]). (**A**) The Rodinia supercontinent at its maximum expansion (1000–850 Ma); (**B**) late Neoproterozoic-Early Paleozoic spreading of the Qilian Ocean; (**C**) collision of the Qilian and Alxa blocks and closure of the Qilian Ocean; (**D**) progressive closure of the Paleo-Tethys Ocean and exhumation of the Qilian Shan; (**E**) the collision of the Lhasa plate with Eurasia caused the exhumation of Qilian Shan during the Early Cretaceous; (**F**) the Indian plate collided with Eurasia in the early Cenozoic and caused the exhumation of Qilian Shan. The red star marks the position of the Qilian Block.

The Paleozoic Qilian Shan orogen was reactivated by the far-field effects of block collisions along the southern edge of the Asian continent, especially that of the Qiangtang and Lhasa blocks, respectively during the Permo-Triassic [76,79–81] and Early Cretaceous [2,7,82–84] (Figure 3E). This renewed tectonic activity led to erosion and deposition of Permo-Triassic and Cretaceous coarse clastic sediments in the piedmont of the North Qilian Shan that was extending up to the present-day upper reaches of the Hei River [7,18,21] (Figure 1C). Low-temperature thermochronological studies indicate that pulses of exhumation occurred in the North Qilian Shan from west to east during the Triassic and Early Cretaceous [2,32,85]. Therefore, the Mesozoic tectonic reactivation was characterized by contractional deformation, resulting in shortening and thickening within the North Qilian Shan during these periods [2,18,22,86]. The Cenozoic deformation and uplift of the North Qilian Shan is recorded in the Jiuquan and Minle foreland basins (Figures 1 and 3F): from Eocene-Oligocene onward, coarse clastic sediments were deposited with increasing sedimentation rates and several angular unconformities [48,87] (Figure 4).

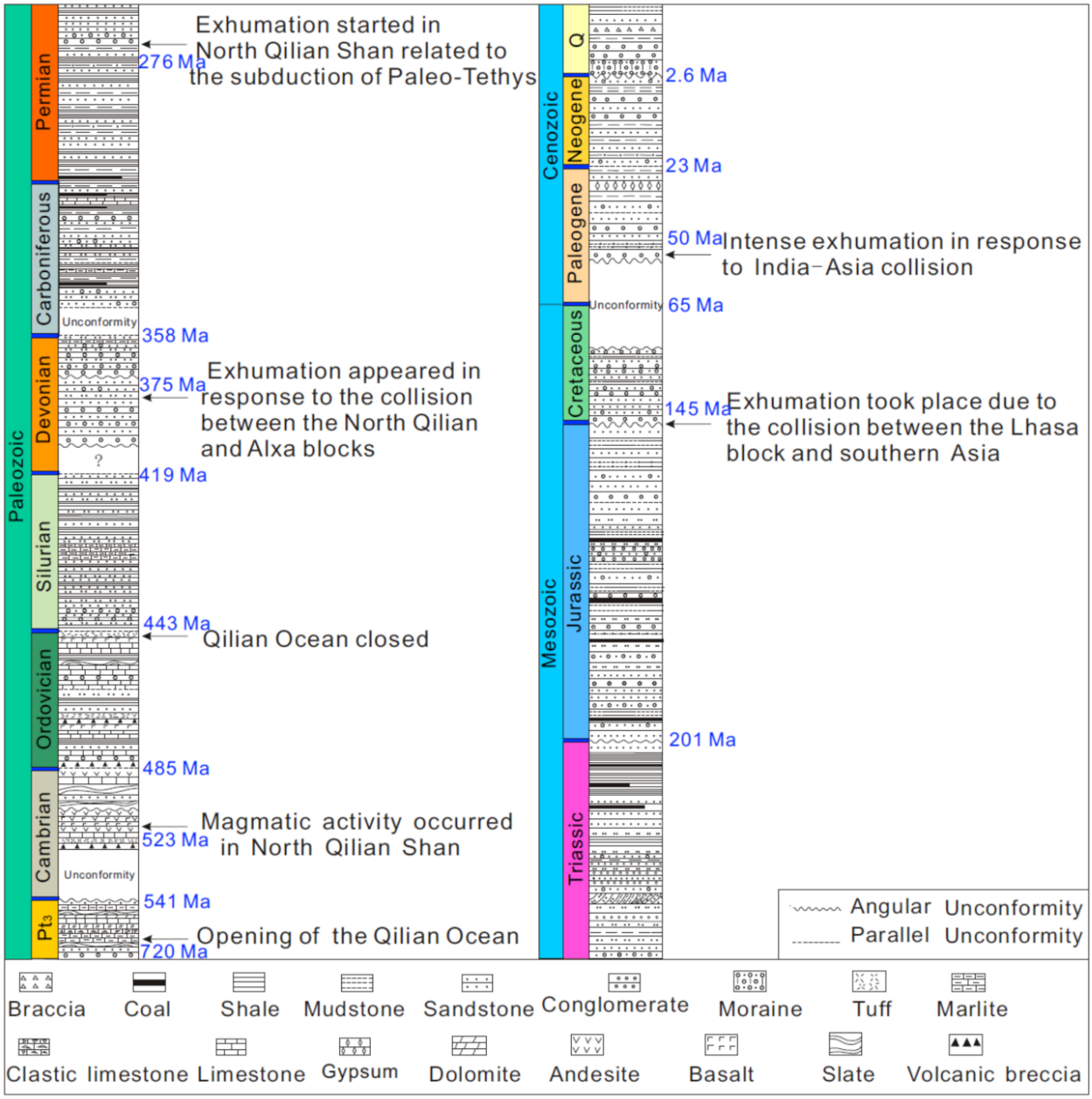

Figure 4. Regional stratigraphy and tectonic evolution in the North Qilian Shan ([6,33,88,89]).

2.2. Hei River

The Hei River is the second-largest endorheic fluvial system in NW China (Figure 1B). The upper reaches of the river are composed of a western tributary and an eastern tributary that merge near Qilian city. The western tributary is the main stream flowing from the North Qilian Shan over a distance of 208 km until the confluence in Qilian city [30]. It then flows into the Hexi Corridor where it largely disappears in the desert. The eastern tributary, the Babao River, originates from the eastern parts of the North Qilian Shan. With a length of 106 km, it ultimately joins the upper reaches of the Hei River near Qilian city. The total length of the Hei River exceeds 821 km, with a drainage area of about 130,000 km^2 [90].

U-Pb analysis of detrital zircons from modern river-bed sands has become an effective tool for provenance studies, comparing the U-Pb age statistical distribution in sand samples with the known zircon U-Pb ages of bedrock in the drainage system [91]. Detrital zircon grains from rivers in the western parts of the North Qilian Shan (location 1 on Figure 1B) yielded five major U-Pb peak ages at 273 Ma, 462 Ma, 756 Ma, 1835 Ma and 2440 Ma [92] (Figure 5a). Detrital zircons found in the river sediments from the central parts of the North Qilian Shan (location 2 on Figure 1B) can again be divided into five major U-Pb peak ages at 267 Ma, 443 Ma, 973 Ma, 1776 Ma and 2481 Ma [93] (Figure 5b). Detrital zircons from the Hei River (locations 3 on Figure 1B) still show five major U-Pb peak ages at 270 Ma, 450 Ma, 950 Ma, 1850 Ma and 2450 Ma, lacking the 756 Ma peak observed in the western North Qilian Shan River [91] (Figure 5c). The bedrock samples from North Qilian Shan have zircon U-Pb age distributions that can be generally divided into five peaks: 2500 Ma, 1800 Ma, 900 Ma, 750 Ma, 440 Ma, and 270 Ma [6,35,36,90] (Figure 5d). These peaks are largely similar to the peaks observed in the detrital zircon U-Pb ages. Detrital zircon U-Pb age populations obtained from compiling the whole North Qilian Shan sediment studies are thus consistent with the U-Pb ages reported from basement rocks cropping out along the modern North Qilian orogenic belt. This result assesses the geographic large-scale representativity of detrital ages in the modern rivers of the North Qilian Shan relative to the existing sources [60,63,64]. However, it seems that the Hei River does not reach the 756 Ma source observed in the western North Qilian Shan River.

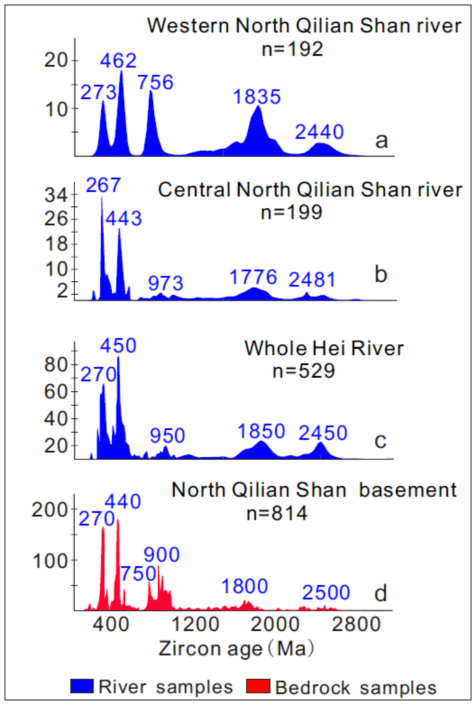

Figure 5. Comparison of the U-Pb age peaks of detrital river zircon grains from Western North Qilian Shan ((**a**), [92]), Central North Qilian Shan ((**b**), [93]), whole Hei River ((**c**), [90]) with those from the North Qilian Shan ((**d**), [6,35,36,90]).

3. Methods and Materials

Ten samples composed of ~3–5 kg of sand were collected from the upper Hei river, the Babao river, and various affluents for detrital ZFT analysis (Figure 6). Following mineral separation through conventional methods, zircon grains were mounted in Teflon sheets and polished using aluminum oxides (powder granulometries of 3.0 µm and 0.3 µm) to expose internal grain surfaces. As we did no obtain enough zircon crystals to mount several aliquots [68,94–96], spontaneous fission tracks were revealed using chemical etching in an eutectic mixture of NaOH and KOH during 18 h at 225 °C [68,94–97]. The revealed spontaneous fission-tracks were counted using a full automated Leica DM6M microscope with nominal magnification of 1000×. Zircon fission-track ages were calibrated using Fish Canyon Tuff (FCT) as an age standard [98]. Uranium content was measured using a quadrupole ICP-MS Agilent 7800 coupled with a UP213 nm New Wave Research Laser Ablation system at Chronus Camp Research-Thermochronology Laboratory facilities, Brazil [99]. A laser ablation spot diameter between 30 µm and 40 µm was chosen to cover the area over which spontaneous fission tracks were counted. The fission-track ages were calculated using the scheme presented by Donelick [100] using a modified zeta calibration approach [101,102].

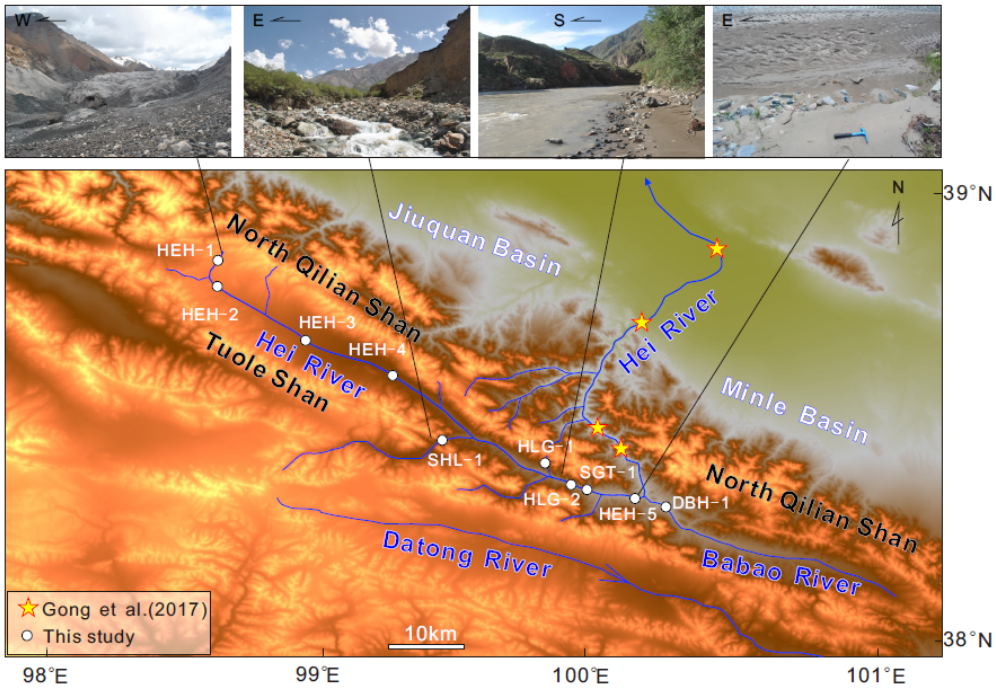

Figure 6. Sampling locations for available detrital zircon U-Pb (stars, [90]) and ZFT (circles, this study) data in the Hei River drainage. The color of the stars and circle refer to the different studies.

4. Results

The locations of the samples are shown in Figure 6, and their GPS coordinates are listed in Table 1. Statistical analysis of detrital zircon fission track data ideally requires dating 100–50 zircon grains per sample [103]. However, due to the numerous metamict grains, zircons with strong U-zoning, fractures, and crystals presenting areas too small to be counted [61], only between 24 and 6 grains could be analyzed in each sample. To allow a robust statistical analysis we combined all zircon single-grain FT ages into a single data-set and calculated ZFT age populations using the Density Plotter software [104]. This approach provided a thermochronological signal integrated over the c.a. 8000 km^2 of the Hei River upper drainage system (Figure 6).

The ZFT single ages are widely distributed between about 1200 Ma and about 40 Ma, implying that a large part of the geological history of the range is preserved within the medium-temperature thermal range (Figure 7). Note that the mean error on individual ages

is of 35% implying that the oldest ages (especially Proterozoic) may sometimes be poorly defined. The Proterozoic ages represent 33% of the total amount of data. A first group of a few late Mesoproterozoic ages displays a statistically relevant peak age (composed of at least three individual ages) at 1057 Ma. The Neoproterozoic ages are distributed between 900 Ma and 550 Ma with individual peaks at 900 Ma, 800 Ma, and 588 Ma. While the 900 Ma peak is represented by a small number of ages, the 800 Ma peak is clearly discernible, possibly corresponding to a single geological event. The youngest ages are largely spread between 750 Ma and 550 Ma with a higher density of Ediacarian ages corresponding to the 588 Ma peak. Paleozoic ages are representing the higher proportion (46%) of the total amount of data. Early Paleozoic ages are mostly clustering between two peaks in the Cambrian and Ordovician at 523 Ma and 450 Ma while the Late Paleozoic ages show two peaks in the Devonian and Permian at 375 Ma and 275 Ma. Mesozoic ages, representing 19% of the total number of data, are displaying a well-constrained peak at 145 Ma. Finally, the Cenozoic data are only represented by four ages (2% of the total number of data) form a poorly defined population peaking at 50 Ma. The detailed FT analytical results of the detrital zircons are listed in Supplementary Table S1.

Table 1. Collected detrital ZFT samples.

Sample Number	Latitude	Longitude	Number of Single-Grain Ages
HEH-1	38°16′14″	99°52′54″	20
HEH-2	38°54′05″	98°48′15″	18
HEH-3	38°37′06″	99°20′53″	17
HEH-4	38°24′24″	99°38′46″	16
SHL-1	39°29′43″	96°31′29″	7
HLG-1	38°15′06″	99°52′29″	21
HLG-2	38°15′04″	99°52′56″	21
STG-1	38°16′17″	99°53′12″	6
HEH-5	38°13′20″	100°10′57″	24
DBH-1	38°13′20″	100°11′03″	19

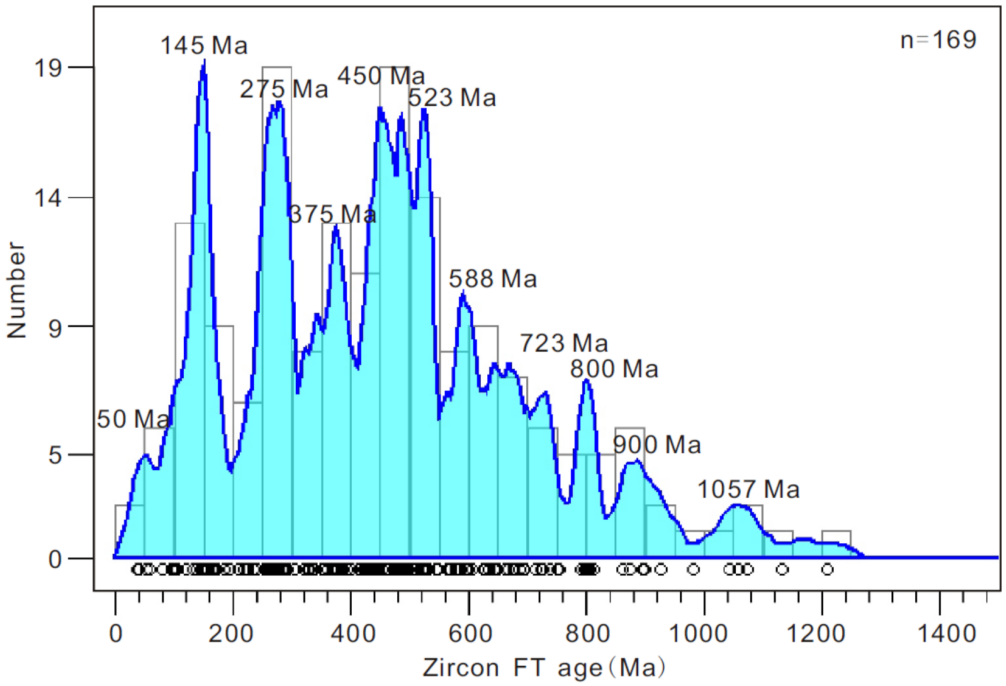

Figure 7. Kernel analysis histogram of all individual ZFT ages obtained from the Hei River. Calculated using the Density Plotter software (Version 8.5, Vermeesch, P, London, UK, https://www.ucl.ac.uk/~ucfbpve/densityplotter/, accessed on 25 February 2022) [104]. Raw analytical data are available as "Supplement Table S1" to this article.

5. Discussion

Compiling the new ZFT data presented above and the detrital zircon U-Pb data available in the bibliography, we discuss the various tectono-metamorphic events that affected the North Qilian Shan since the Proterozoic. A specific focus is made on deciphering the Mesozoic events from the Cenozoic one.

5.1. The Meso-Neoproterozoic and Paleozoic Magmatic Activity

The late Mesoproterozoic to early Neoproterozoic ZFT ages, including the peaks at 1057 Ma and 900 Ma relate to the assembly of the Rodinia supercontinent (Figures 8A and 9A). Zircon U-Pb ages obtained from the basement and fluvial sediments of the North Qilian Shan indeed record magmatism during this period [90] (Figure 8B). It should be noted that an older zircon U-Pb age population at 2500 Ma is not represented in the ZFT ages [6,35,36,90] (Figure 5d). The ZFT ages do not match the Archean zircon U-Pb age peaks, which conventional interpretation would ascribe to the likelihood of sediment recycling [39]. Similar Proterozoic zircon U-Pb ages have been obtained over most of the Qilian Shan (see Section 2.1) [43,105–108]. Widespread late Mesoproterozoic-early Neoproterozoic magmatic activity also occurred in the Alxa block [109,110], the Tarim Craton [111,112], and the South China Craton [113,114], in relation with the construction of the Rodinia supercontinent [115] (Figure 3A). In that framework, we interpret the Proterozoic detrital ZFT age populations in the Hei River basin as recording the accretion of the North Qilian block to the Rodinia supercontinent.

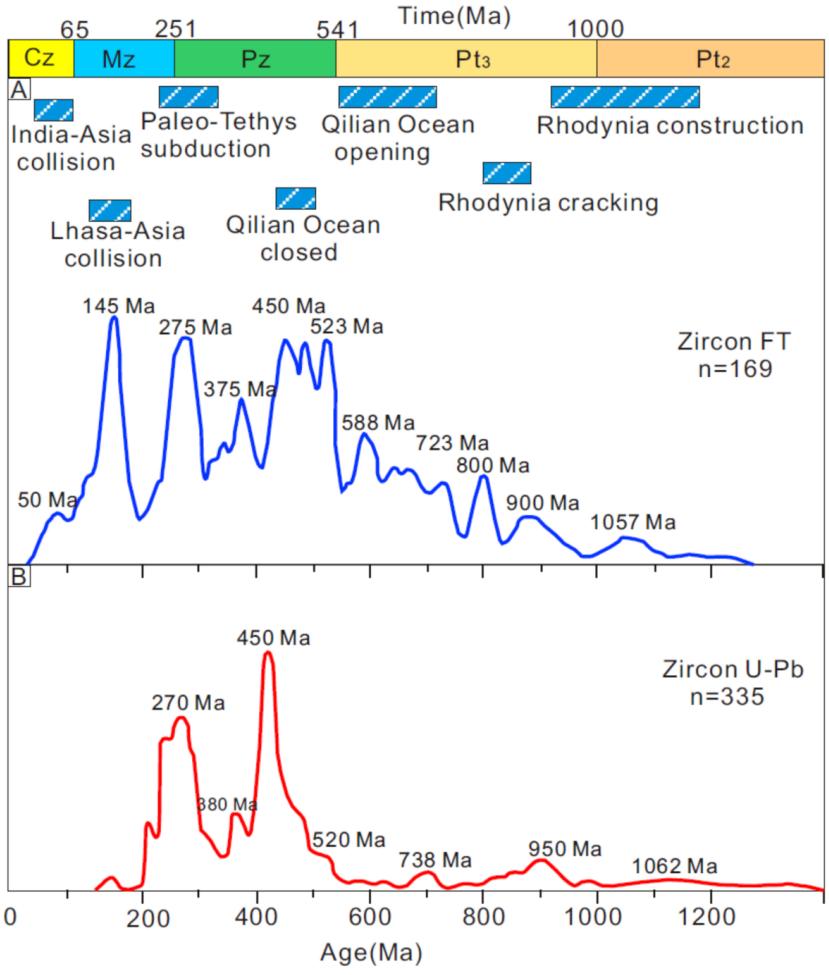

Figure 8. (**A**) Frequency distribution of detrital zircon fission track ages in the upper reaches of the Hei River. (**B**) U-Pb age frequency distribution of Middle Proterozoic and Mesozoic detrital zircons in the Hei River basin. Data source: [90].

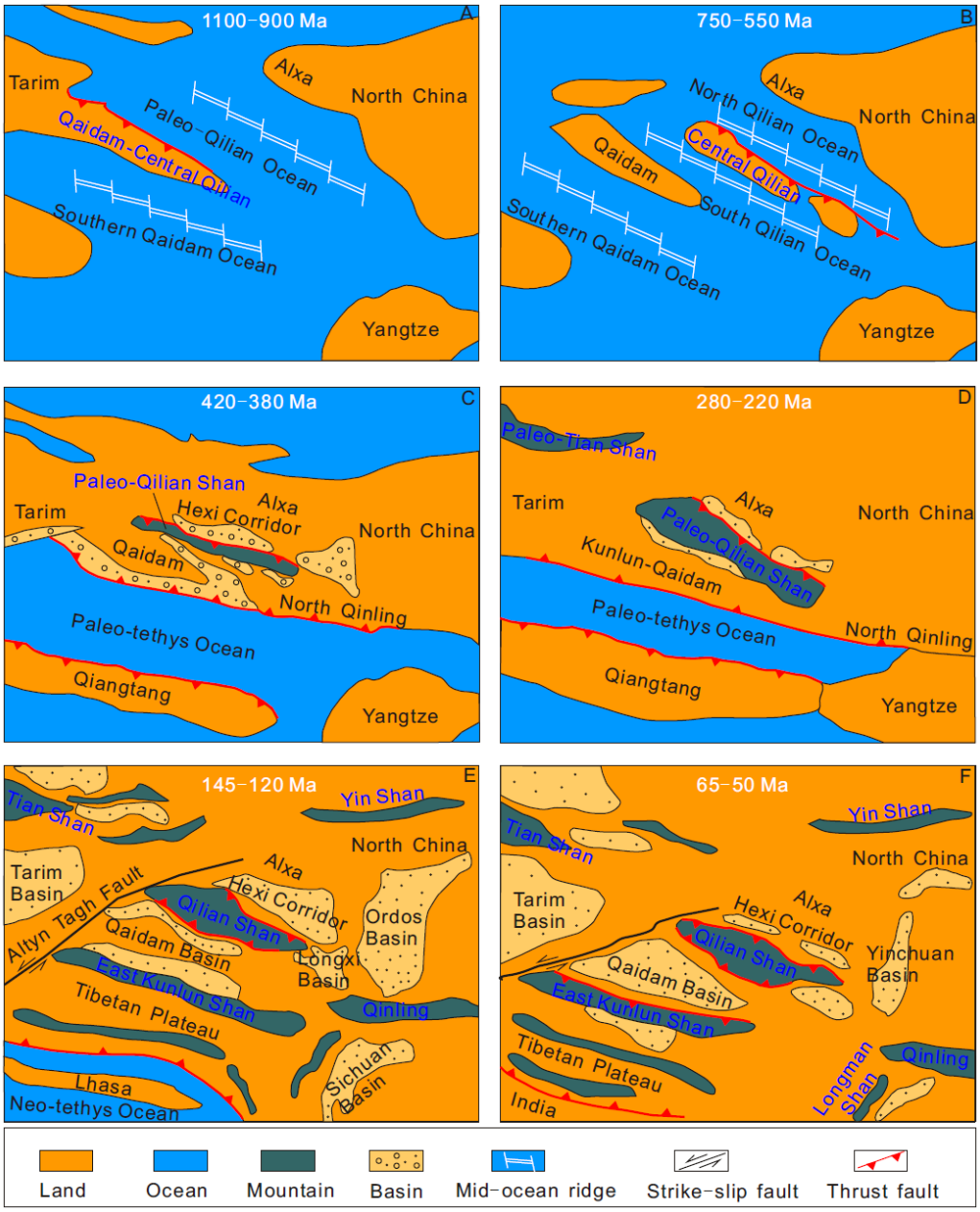

Figure 9. (**A**–**F**) Tectonic evolution of the Qilian orogenic belts from the onset of the Neoproterozoic to the early Cenozoic (Modified from [7,75,81,116]).

The detrital ZFT age population at 800 Ma documents the magmatic-thermal rifting activity and onset of opening of the Qilian Ocean in the North Qilian Shan. This rifting phase was associated to granite intrusions as reflected by the U-Pb ages of bedrock and detrital zircons in the Hei River basin [90], and North [6,7,36], Central [107] and South Qilian basements [117]. During that same period, simultaneous magmatic activities took place in the Alxa, Tarim, and Yangtze blocks, in relation with the breakup of the Rodinia supercontinent [7,8,75,116,118,119].

The late Neoproterozoic zircons with fission track ages ranging from about 750 Ma to 550 Ma, including the peak age at 588 Ma are consistent with the timing of the opening and spreading of the Qilian Ocean (Figure 9B). Oceanic spreading was accompanied by extensive volcanism recorded in the whole Qilian Shan orogen [6,7,43,90,107,117]. The results presented above imply that some of those magmatic zircons have remained in the upper crust (above 8 to 10 km depth) since the late Mesoproterozoic and avoided fission track annealing during the following tectonic and metamorphic events. This in turn suggests

that both the Late Proterozoic and Paleozoic orogenic events that took place in the Qilian Shan region remained limited in terms of metamorphism and crustal exhumation.

It is generally considered that the subduction and closure of the North Qilian Ocean and subsequent continent-continent collision between the North Qilian Block and Alxa Block occurred in the early Paleozoic [6,73] and that the Qilian Ocean was fully closed at 440–450 Ma [6,7,33,107,120] (Figures 9C and 10A). The early Paleozoic ZFT ages including the two peaks at 523 Ma and 450 Ma are directly associated to that final closure of the Qilian Ocean (Figure 8A). The peak age at about 450 Ma is also strongly represented in the detrital U-Pb data as well as in the basement zircon U-Pb data (Figure 5d). Since older, Proterozoic ages have been preserved in the range, implying a low limited post-Proterozoic exhumation, this suggests that the granitoids associated to that initial phase of collision where emplaced within the upper-crust and cooled down rapidly to less than 250 °C. However, the continent-continent collision between the North Qilian and Alxa blocks lasted until late Silurian-early Devonian (420–380 Ma, [72]), as indicated by the Silurian flysch deposits that shift to Devonian molasse rocks in the Hexi Corridor [6,7,33,121]. The samples collected in the Hei River system contain Devonian to Early Carboniferous ZFT ages (with a peak age at 375 Ma), which recorded that long-lasting collision. A similar zircon U-Pb peak age (380 Ma) has been reported from the Hei River basin ([90], Figure 8B), which indicates that ZFT ages again correspond to granitoid emplacement and not to a strong exhumation event.

The well-marked ZFT population peaking at 275 Ma indicates a Late Paleozoic event. The late Paleozoic magmatic and sedimentary series from the southernmost part of the Alxa block yield relatively consistent early Permian apatite U-Pb and FT ages ranging from 276 Ma to 290 Ma [122]. In addition, ZFT and AFT results from the western part of the North Qilian Shan document magmatic event that occurred at 270–250 Ma [9,85]. This signal can also be found in the detrital zircons U-Pb ages (270 Ma) from the whole Hei River drainage [90]. Zircon (U-Th)/He and AFT ages reveal that the emplacement of the Heli Shan and the Longshou Shan granitoids occurred at 275 Ma and 277 Ma, respectively [123]. The subduction of the Paleo-Tethys oceanic lithosphere separating the Qaidam-Qilian-Alxa Block from the Qiangtang Block occurred during the Late Carboniferous-Triassic period (300–220 Ma, [21,77,81,107,124–126]) (Figure 9D). These results indicate that magmatism occurred widely in the South, Central and North Qilian Shan and Alxa block during this time.

5.2. Early Cretaceous Cooling

Although, Mesozoic detrital zircon U-Pb ages are rare in the Hei River sediments [90], bedrock AFT and ZFT ages constrain rapid Early Cretaceous exhumation in the Qilian Shan and surrounding regions, including the North Qilian Shan (140–123 Ma [2,85]), the Longshou Shan (110 Ma [127]), the Hei Shan (135 Ma [25]), the Altun Shan (120 Ma [128]), the Helan Shan (125 Ma [129]) or the southern part of Alxa block (145 Ma [122], Figure 10B). This is further confirmed by the detrital ZFT age peak of 145 Ma obtained in this study as well as detrital AFT data from the eastern part of the North Qilian Shan [20,130]. Vincent and Allen [18] and Chen et al. [84] described Early Cretaceous conglomerates and coarse sediments exposed in the Hexi Corridor and Jiuquan Basin, derived from renewed erosion in the North Qilian Shan. Sandstone petrography and detrital zircon provenance analysis in the Yumen basin further documented Early Cretaceous initiation of relief building in the North Qilian Shan [86,131,132] (Figure 10). The Lhasa-Qiangtang collision along the Bangong-Nujiang suture zone in Tibet [83,133] (Figure 9E) and possibly the final closure of the Mongol-Okhotsk Ocean [134–136] (Figure 3E) during the Early Cretaceous (145–130 Ma), have been inferred to play a major role on the late Mesozoic tectonic exhumation in northern Tibet and the adjacent regions [82,85,122,123,137]. However, the regions of strong exhumation were probably localized along major thrust fault, in a setting similar to that of the present-day deformation. Indeed, once again the preservation of the Proterozoic and Paleozoic ZFT ages as well as of the early to middle Mesozoic AFT ages [2,9,85], imply that not all of the range was affected by exhumation. This seems to be a recurrent tectonic pattern since at least the Paleozoic collision of the Qilian and Alxa blocks.

5.3. Early Cenozoic Exhumation of the North Qilian Shan

Enclosed by the rigid backstops formed by the Tarim block to the west, the western Qinling orogenic belt to the east, and the Alxa Block-North China Craton to the north, the Cenozoic Qilian orogenic belt has been affected by intense contraction driven by the continuous subduction of the Indian plate beneath the Asian continent [1]. The Cenozoic deformation pattern was at least partly controlled by the Paleozoic-Mesozoic inherited fabrics [2,9,22,24,30,31,47].

A growing set of data points toward an early Eocene onset of deformation and exhumation as a first likely response to far-field effects of the India-Asia collision [14,31,48,81,87,138] (Figure 9F). In the Yumen and Jiuquan basins, late Lutetian to early Bartonian coarse clastic sediments deposited in alluvial fan and braided river environments are separated from the underlying Upper Cretaceous strata by an angular unconformity indicating tectonic movement around or prior to 40 Ma ([48,87], Figure 10B). By that time, the Hexi Corridor was mainly filled by clastic material derived from the erosion of the North Qilian Shan. To the south, the thick conglomerate beds of the early Eocene Lulehe Formation are widely found along the margins of the North Qaidam Basin [13,139]. Bedrock apatite FT ages from the North Qilian Shan largely cluster at 52–47 Ma [22,138,140]. This is consistent with the few ZFT data around 50 Ma observed in this study. Similar evidence of Eocene exhumation has been reported from the South Qilian Shan [28,141], the Central Qilian Shan [137,142], eastern Kunlun Shan [143,144], and western Qinling Shan [145].

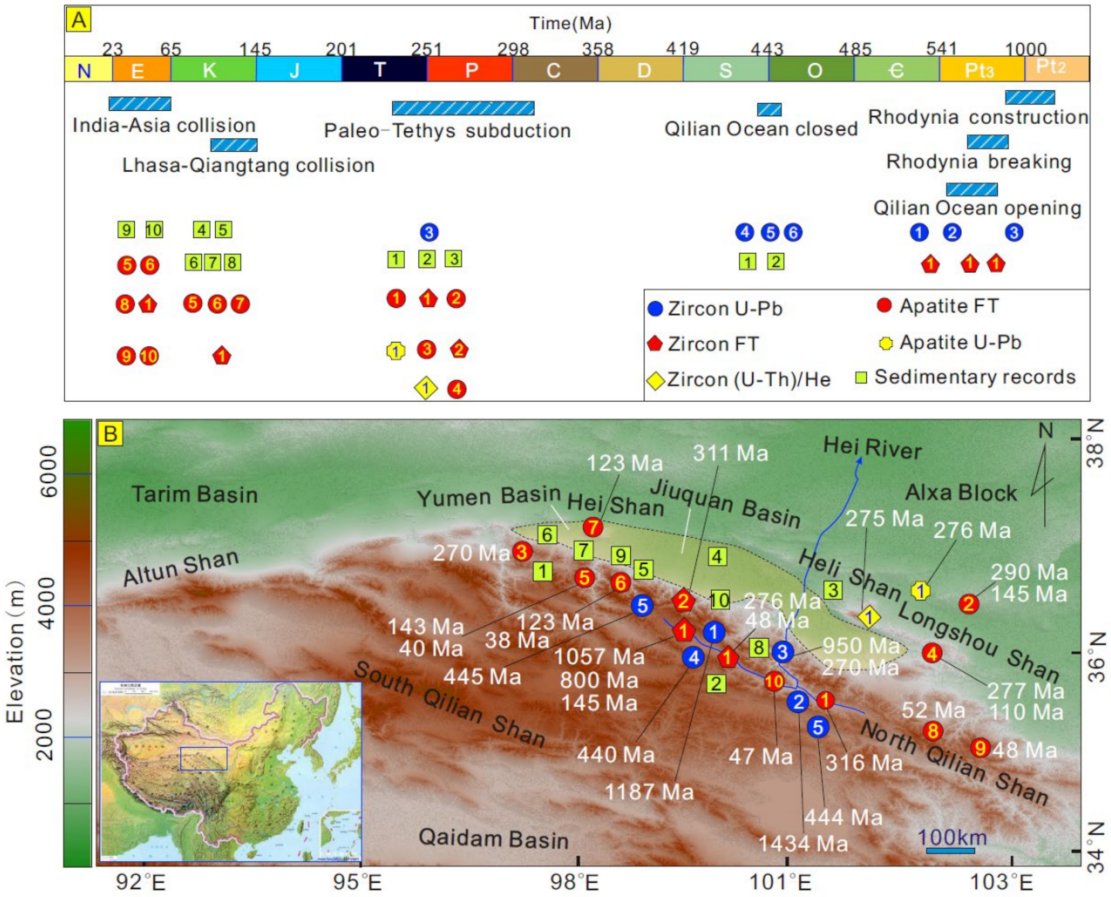

Figure 10. (**A**) Temporal distribution plot of tectonic-related events recorded in the North Qilian Shan, as constrained by zircon U-Pb, FT, and (U-Th)/He ages, apatite FT and U-Pb ages, and sedimentary records. (**B**) The specific distribution of the study sites in the North Qilian Shan, data source: zircon U-Pb ages, 1: [6]), 2: [36], 3: [90], 4: [107], 5: [7], 6: [32]; zircon FT ages, 1: This study, 2: [85]; zircon (U-Th)/He age, 1: [123]; apatite FT ages: 1: [30], 2: [122], 3: [9], 4: [127], 5: [1], 6: [85], 7: [128], 8: [140], 9: [22], 10: [144]; apatite U-Pb ages, 1: [122]; Sedimentary records, 1: [7], 2: [107], 3: [123], 4: [18], 5: [82], 6: [131], 7: [132], 8: [86]; 9: [48], 10: [87].

6. Conclusions

Our modern-river sand detrital zircon fission track data from the upper reaches of Hei River along the North Qilian Shan, provides a better understanding of the tectono-geomorphological evolution of the North Qilian Shan from the late Proterozoic to the Cenozoic. Strong post-magmatic cooling events occurred in the North Qilian Shan during the late Mesoproterozoic—early Neoproterozoic, corresponding to the assembly of the Rodinia supercontinent. The detrital zircon fission track age population at 800 Ma documents the onset of oceanic spreading in the late Neoproterozoic and the initial dismantling of Rodinia. ZFT ages ranging from about 750 Ma to 550 Ma (with peak ages at 723 Ma and 588 Ma) are consistent with the timing of the opening and spreading of the Qilian Ocean, while the early Palaeozoic ages (including the Cambrian peak at 523 Ma and the Ordovician peak at 450 Ma) mark the progressive closure of that ocean ending with the collision of the Qilian block with the Alxa block—North China craton in the Devonian. The Qilian Ocean finally closed at Late Devonian (375 Ma). In the late Paleozoic (275 Ma), the subduction of the Paleo-Tethys Ocean played a leading role in the magmatism of the North Qilian Shan. During the Lower Cretaceous (145 Ma), the accretion of the Lhasa block to the south (and potentially the closure of the Mongol-Okhotsk Ocean to the northeast) triggered a renewed tectonic activity in the Qilian Shan. Finally, an early Eocene exhumation event (50 Ma) suggests that the NE Tibetan Plateau started to deform nearly synchronously with the onset of India-Asia collision. Finally, the preservation of the Proterozoic and early Paleozoic ZFT ages in the range suggest that regional exhumation remained limited during the Paleozoic, Mesozoic, and Cenozoic events. We infer that, similarly to the Cenozoic setting, exhumation was localized along major compressive structures, preserving large areas from erosion and exhumation. This further attests of the importance of inherited structures in the evolution of intra-continental orogens.

Supplementary Materials: The following supporting information can be downloaded at: https://www.mdpi.com/article/10.3390/geosciences12040166/s1. Table S1.

Author Contributions: Conceptualization, X.L. and J.M.; methodology, L.L.; software, J.C.; validation, X.L. and J.M.; formal analysis, X.L.; investigation, X.L.; resources, X.L.; data curation, X.L. and J.M.; writing—original draft preparation, X.L., J.M., J.L.-Z., F.C., Z.W. and Y.T.; writing—review and editing, X.L. and J.L.-Z.; funding acquisition. All authors have read and agreed to the published version of the manuscript.

Funding: This work was financially supported by the National Natural Science Foundation of China (Grant 41972212, 42030305), and Research Foundation of Chutian Scholars Program of Hubei Province (No. 8210403).

Data Availability Statement: All the data in this study can be accessed in the Supporting Information appeared as the Supplementary Materials.

Acknowledgments: We are exceedingly grateful to some people for them very thoughtful and constructive criticism on earlier versions. We would like to express our gratitude to the two anonymous reviewers whose suggestions and questions were very important to the improvement of the paper.

Conflicts of Interest: The authors declare no conflict of interest.

References

1. Yin, A.; Harrison, T.M. Geologic Evolution of the Himalayan-Tibetan Orogen. *Annu. Rev. Earth Planet. Sci.* **2000**, *28*, 211–280. [CrossRef]
2. Jolivet, M.; Brunel, M.; Seward, D.; Xu, Z.; Yang, J.; Roger, F.; Tapponnier, P.; Malavieille, J.; Arnaud, N.; Wu, C. Mesozoic and Cenozoic tectonics of the northern edge of the Tibetan plateau: Fission-track constraints. *Tectonophysics* **2001**, *343*, 111–134. [CrossRef]
3. Yang, J.; Xu, Z.; Zhang, J.; Chu, C.-Y.; Zhang, R.; Liou, J.-G. Tectonic significance of early Paleozoic high-pressure rocks in Altun-Qaidam-Qilian Mountains, northwest China. *Geol. Soc. Am. Mem.* **2001**, *194*, 151–170. [CrossRef]
4. Xu, Z.; Yang, J.; Wu, C.; Li, H.; Zhang, J.; Qi, X.; Song, S.; Qiu, H. Timing and mechanism of formation and exhumation of the Northern Qaidam ultrahigh-pressure metamorphic belt. *J. Asian Earth Sci.* **2006**, *28*, 160–173.

5. Xiao, W.; Windley, B.F.; Yong, Y.; Yan, Z.; Yuan, C.; Liu, C.-Z.; Li, J. Early Paleozoic to Devonian multiple-accretionary model for the Qilian Shan, NW China. *J. Southeast Asian Earth Sci.* **2009**, *35*, 323–333. [CrossRef]
6. Song, S.; Niu, Y.; Su, L.; Xia, X. Tectonics of the North Qilian orogen, NW China. *Gondwana Res.* **2013**, *23*, 1378–1401. [CrossRef]
7. Zuza, A.V.; Wu, C.; Reith, R.C.; Yin, A.; Li, J.; Zhang, J.; Zhang, Y.; Wu, L.; Liu, W. Tectonic evolution of the Qilian Shan: An early Paleozoic orogen reactivated in the Cenozoic. *GSA Bull.* **2017**, *130*, 881–925. [CrossRef]
8. Yu, S.; Peng, Y.; Zhang, J.; Li, S.; Santosh, M.; Li, Y.; Liu, Y.; Gao, X.; Ji, W.; Lv, P.; et al. Tectono-thermal evolution of the Qilian orogenic system: Tracing the subduction, accretion and closure of the Proto-Tethys Ocean. *Earth-Sci. Rev.* **2021**, *215*, 103547. [CrossRef]
9. George, A.; Marshallsea, S.J.; Wyrwoll, K.-H.; Jie, C.; Yanchou, L. Miocene cooling in the northern Qilian Shan, northeastern margin of the Tibetan Plateau, revealed by apatite fission-track and vitrinite-reflectance analysis. *Geology* **2001**, *29*, 939–942. [CrossRef]
10. Yin, A.; Rumelhart, P.E.; Butler, R.; Cowgill, E.; Harrison, T.M.; Foster, D.A.; Ingersoll, R.V.; Qing, Z.; Xian, Z.; Xiao, W.; et al. Tectonic history of the Altyn Tagh fault system in northern Tibet inferred from Cenozoic sedimentation. *Geol. Soc. Am. Bull.* **2002**, *114*, 1257–1295. [CrossRef]
11. Lease, R.; Burbank, D.W.; Clark, M.K.; Farley, K.; Zheng, D.; Zhang, H. Middle Miocene reorganization of deformation along the northeastern Tibetan Plateau. *Geology* **2011**, *39*, 359–362. [CrossRef]
12. Duvall, A.R.; Clark, M.K.; Kirby, E.; Farley, K.A.; Craddock, W.H.; Li, C.; Yuan, D.-Y. Low-temperature thermochronometry along the Kunlun and Haiyuan Faults, NE Tibetan Plateau: Evidence for kinematic change during late-stage orogenesis. *Tectonics* **2013**, *32*, 1190–1211. [CrossRef]
13. Cheng, F.; Garzione, C.N.; Jolivet, M.; Guo, Z.; Zhang, D.; Zhang, C.; Zhang, Q. Initial Deformation of the Northern Tibetan Plateau: Insights from Deposition of the Lulehe Formation in the Qaidam Basin. *Tectonics* **2019**, *38*, 741–766. [CrossRef]
14. He, P.; Song, C.; Wang, Y.; Meng, Q.; Wang, D.; Feng, Y.; Chen, L.; Feng, W. Early Cenozoic exhumation in the Qilian Shan, northeastern margin of the Tibetan Plateau: Insights from detrital apatite fission track thermochronology. *Terra Nova* **2020**, *32*, 415–424. [CrossRef]
15. Lin, X.; Jolivet, M.; Liu-Zeng, J.; Cheng, F.; Tian, Y.; Li, C.A. Mesozoic-Cenozoic cooling history of the Eastern Qinghai Nan Shan (NW China): Apatite low-temperature thermochronology constraints. *Palaeogeogr. Palaeoclim. Palaeoecol.* **2021**, *572*, 110416. [CrossRef]
16. Jolivet, M.; Cheng, F.; Zuza, A.V.; Guo, Z.; Dauteuil, O. Large-scale topography of the North Tibetan ranges as a proxy to contrasted crustal-scale deformation modes. *J. Geol. Soc.* **2022**. [CrossRef]
17. Meyer, B.; Tapponnier, P.; Bourjot, L.; Métivier, F.; Gaudemer, Y.; Peltzer, G.; Shunmin, G.; Zhitai, C. Crustal thickening in Gansu-Qinghai, lithospheric mantle subduction, and oblique, strike-slip controlled growth of the Tibet plateau. *Geophys. J. Int.* **1998**, *135*, 1–47. [CrossRef]
18. Vincent, S.J.; Allen, M.B. Evolution of the Minle and Chaoshui Basins, China: Implications for Mesozoic strike-slip basin formation in Central Asia. *GSA Bull.* **1999**, *111*, 725–742. [CrossRef]
19. Horton, B.K.; Dupontnivet, G.; Zhou, J.; Waanders, G.L.; Butler, R.F.; Wang, J. Mesozoic-Cenozoic evolution of the Xining-Minhe and Dangchang basins, northeastern Tibetan Plateau: Magnetostratigraphic and biostratigraphic results. *J. Geophys. Res. Earth Surf.* **2004**, *109*, B04402. [CrossRef]
20. Lin, X.B.; Chen, H.; Wyrwoll, K.H.; Batt, G.E.; Liao, L.; Xiao, J. The uplift history of the Haiyuan-Liupan Shan region northeast of the present Tibetan Plateau: Integrated constraint from stratigraphy and thermochronology. *J. Geol.* **2011**, *119*, 372–393. [CrossRef]
21. Cheng, F.; Jolivet, M.; Guo, Z.; Lu, H.; Zhang, B.; Li, X.; Zhang, D.; Zhang, C.; Zhang, H.; Wang, L.; et al. Jurassic-early Cenozoic tectonic inversion in the Qilian Shan and Qaidam Basin, North Tibet: New insight from seismic reflection, isopach mapping and drill core data. *J. Geophys. Res. Solid Earth* **2019**, *124*, 12077–12098. [CrossRef]
22. Li, B.; Zuza, A.V.; Chen, X.; Hu, D.; Shao, Z.; Qi, B.; Xiong, X. Cenozoic multi-phase deformation in the Qilian Shan and out-of-sequence development of the northern Tibetan Plateau. *Tectonophysics* **2020**, *782*, 228423. [CrossRef]
23. Zheng, D.; Clark, M.K.; Zhang, P.; Zheng, W.; Farley, K. Erosion, fault initiation and topographic growth of the North Qilian Shan (northern Tibetan Plateau). *Geosphere* **2010**, *6*, 937–941. [CrossRef]
24. Pan, B.; Li, Q.; Hu, X.; Gao, H.; Li, Z. Cretaceous and Cenozoic cooling history of the eastern Qilian Shan, north-eastern margin of the Tibetan Plateau: Evidence from apatite fission-track analysis. *Terra Nova* **2013**, *25*, 431–438.
25. An, K.; Lin, X.; Wu, L.; Yang, R.; Chen, H.; Cheng, X.; Xia, Q.; Zhang, F.; Ding, W.; Gao, S.; et al. An immediate response to the Indian-Eurasian collision along the northeastern Tibetan Plateau: Evidence from apatite fission track analysis in the Kuantan Shan-Hei Shan. *Tectonophysics* **2019**, *774*, 228278. [CrossRef]
26. Tong, K.; Li, Z.; Zhu, L.; Tao, G.; Zhang, Y.; Yang, W.; Zhang, J. Fold-and-thrust deformation of the hinterland of Qilian Shan, northeastern Tibetan Plateau since Mesozoic with implications for the plateau growth. *J. Southeast Asian Earth Sci.* **2019**, *198*, 104131. [CrossRef]
27. Yu, J.; Pang, J.; Wang, Y.; Zheng, D.; Liu, C.; Wang, W.; Xiao, L. Mid-Miocene uplift of the northern Qilian Shan as a result of the northward growth of the northern Tibetan Plateau. *Geosphere* **2019**, *15*, 423–432. [CrossRef]
28. Cheng, X.; Lin, X.; Wu, L.; Chen, H.; Xiao, A.; Gong, J.; Yang, S. The Exhumation History of North Qaidam Thrust Belt Constrained by Apatite Fission Track Thermochronology: Implication for the Evolution of the Tibetan Plateau. *Acta Geol. Sin.* **2016**, *90*, 870–883.

29. Zuza, A.V.; Cheng, X.; Yin, A. Testing models of Tibetan Plateau formation with Cenozoic shortening estimates across the Qilian Shan–Nan Shan thrust belt. *Geosphere* **2016**, *12*, 501–532. [CrossRef]
30. Lin, X.; Tian, Y.; Donelick, R.A.; Liu-Zeng, J.; Cleber, S.J.; Li, C.A.; Wu, Q.; Li, Z. Mesozoic and Cenozoic tectonics of the northeastern edge of the Tibetan plateau: Evidence from modern river detrital apatite fission-track age constraints. *J. Southeast Asian Earth Sci.* **2018**, *170*, 84–95. [CrossRef]
31. Cheng, F.; Jolivet, M.; Guo, Z.; Wang, L.; Zhang, C.; Li, X. Cenozoic evolution of the Qaidam basin and implications for the growth of the northern Tibetan plateau: A review. *Earth-Sci. Rev.* **2021**, *220*, 103730. [CrossRef]
32. Li, B.; Zuza, A.V.; Chen, X.; Wang, Z.-Z.; Shao, Z.; Levy, D.A.; Wu, C.; Xu, S.; Sun, Y. Pre-cenozoic evolution of the northern Qilian Orogen from zircon geochronology: Framework for early growth of the northern Tibetan Plateau. *Palaeogeogr. Palaeoclim. Palaeoecol.* **2020**, *562*, 110091. [CrossRef]
33. Xia, L.Q.; Li, X.M.; Yu, J.Y.; Wang, G.Q. Mid-late neoproterozoic to early paleozoic volcanism and tectonic evolution of the Qilianshan, NW China. *GeoResJ* **2016**, *9–12*, 1–41. [CrossRef]
34. Chen, Y.X.; Song, S.G.; Niu, Y.L.; Wei, C.J. Melting of continental crust during subduction initiation: A case study from the Chaidanuo peraluminous granite in the North Qilian suture zone. *Geochim. Cosmochim. Acta* **2014**, *132*, 311–336. [CrossRef]
35. Zhao, L.; Yu, J.; Zhao, J.; Fan, X.; Chen, S. LA-ICP-MS zircon U-Pb age, geochemistry of Chaidano Mountain granite mass in the western part of North Qilian Shan. *Gansu Geol.* **2018**, *27*, 8–16. (In Chinese)
36. Tseng, C.-Y.; Yang, H.-Y.; Yusheng, W.; Dunyi, L.; Wen, D.-J.; Lin, T.-C.; Tung, K.-A. Finding of Neoproterozoic (~775 Ma) magmatism recorded in metamorphic complexes from the North Qilian orogen: Evidence from SHRIMP zircon U-Pb dating. *Chin. Sci. Bull.* **2006**, *51*, 963–970. [CrossRef]
37. Zhang, J.X.; Meng, F.C.; Wan, Y.S. A cold Early Palaeozoic subduction zone in the North Qilian Mountains, NW China: Petrological and U-Pb geochronological constraints. *J. Metamorph. Geol.* **2007**, *25*, 285–304. [CrossRef]
38. Tartèse, R.; Ruffet, G.; Poujol, M.; Boulvais, P.; Ireland, T.R. Simultaneous resetting of the muscovite K-Ar and monazite U-Pb geochronometers: A story of fluids. *Terra Nova* **2011**, *23*, 390–398. [CrossRef]
39. Carter, A.; Bristow, C.S. Detrital zircon geochronology: Enhancing the quality of sedimentary source information through improved methodology and combined U-Pb and fission-track techniques. *Basin Res.* **2000**, *12*, 47–57. [CrossRef]
40. Jolivet, M.; Roger, F.; Xu, Z.Q.; Paquette, J.L.; Cao, H. Mesozoic-Cenozoic evolution of the Danba dome (Songpan-Garzê, east Tibet) as inferred from LA-ICPMS U-Pb and fission-track data. *J. Asian Earth Sci.* **2015**, *102*, 180–204. [CrossRef]
41. Roger, F.; Teyssier, C.; Respaut, J.-P.; Rey, P.; Jolivet, M.; Whitney, D.; Paquette, J.-L.; Brunel, M. Timing of formation and exhumation of the Montagne Noire double dome, French Massif Central. *Tectonophysics* **2014**, *640–641*, 53–69. [CrossRef]
42. Song, S.; Niu, Y.; Zhang, L.; Wei, C.; Liou, J.G.; Su, L. Tectonic evolution of early Paleozoic HP metamorphic rocks in the North Qilian Mountains, NW China: New perspectives. *J. Southeast Asian Earth Sci.* **2009**, *35*, 334–353. [CrossRef]
43. Zhang, S.; Jian, X.; Pullen, A.; Fu, L.; Liang, H.; Hong, D.; Zhang, W. Tectono-magmatic events of the Qilian orogenic belt in northern Tibet: New insights from detrital zircon geochronology of river sands. *Int. Geol. Rev.* **2020**, *63*, 917–940. [CrossRef]
44. Lin, X.; Zheng, D.; Sun, J.; Windley, B.F.; Tian, Z.; Gong, Z.; Jia, Y. Detrital apatite fission track evidence for provenance change in the Subei Basin and implications for the tectonic uplift of the Danghe Nan Shan (NW China) since the mid-Miocene. *J. Southeast Asian Earth Sci.* **2015**, *111*, 302–311. [CrossRef]
45. He, P.; Song, C.; Wang, Y.; Meng, Q.; Chen, L.; Yao, L.; Huang, R.; Feng, W.; Chen, S. Cenozoic deformation history of the Qilian Shan (northeastern Tibetan Plateau) constrained by detrital apatite fission-track thermochronology in the northeastern Qaidam Basin. *Tectonophysics* **2018**, *749*, 1–11. [CrossRef]
46. Wang, W.; Zheng, D.; Li, C.; Wang, Y.; Zhang, Z.; Pang, J.; Wang, Y.; Yu, J.; Wang, Y.; Zheng, W.; et al. Cenozoic Exhumation of the Qilian Shan in the Northeastern Tibetan Plateau: Evidence from Low-Temperature Thermochronology. *Tectonics* **2020**, *39*, e2019TC005705. [CrossRef]
47. He, P.; Song, C.; Wang, Y.; Chen, L.; Chang, P.; Wang, Q.; Ren, B. Cenozoic exhumation in the Qilian Shan, northeastern Tibetan Plateau: Evidence from detrital fission track thermochronology in the Jiuquan Basin. *J. Geophys. Res. Solid Earth* **2017**, *122*, 6910–6927. [CrossRef]
48. Dai, S.; Fang, X.; Song, C.; Gao, J.; Gao, D.; Li, J. Early tectonic uplift of the northern Tibetan Plateau. *Chin. Sci. Bull.* **2005**, *50*, 1642–1652. [CrossRef]
49. Song, C.; Fang, X.; Li, J.; Gao, J.; Zhao, Z.; Fan, M. Tectonic uplift and sedimentary evolution of the Jiuxi Basin in the northern margin of the Tibetan Plateau since 13 Ma BP. *Sci. China Ser. D Earth Sci.* **2001**, *44*, 192–202. [CrossRef]
50. Bovet, P.M.; Ritts, B.D.; Gehrels, G.; Abbink, A.O.; Darby, B.; Hourigan, J. Evidence of Miocene crustal shortening in the North Qilian Shan from Cenozoic stratigraphy of the western Hexi Corridor, Gansu Province, China. *Am. J. Sci.* **2009**, *309*, 290–329. [CrossRef]
51. An, K.; Lin, X.; Wu, L.; Cheng, X.; Chen, H.; Ding, W.; Li, C. Reorganization of sediment dispersal in the Jiuxi Basin at ~17 Ma and its implications for uplift of the NE Tibetan Plateau. *Palaeogeogr. Palaeoclimatol. Palaeoecol.* **2018**, *511*, 558–576. [CrossRef]
52. Shi, W.; Wang, F.; Yang, L.; Wu, L.; Zhang, W. Diachronous Growth of the Altyn Tagh Mountains: Constraints on Propagation of the Northern Tibetan Margin From (U-Th)/He Dating. *J. Geophys. Res. Solid Earth* **2018**, *123*, 6000–6018. [CrossRef]
53. Fang, X.; Liu, D.; Song, C.; Dai, S.; Meng, Q. Oligocene slow and Miocene–Quaternary rapid deformation and uplift of the Yumu Shan and North Qilian Shan: Evidence from high-resolution magnetostratigraphy and tectonosedimentology. *Geol. Soc. Lond. Spéc. Publ.* **2012**, *373*, 149–171. [CrossRef]

54. Hu, X.; Chen, D.; Pan, B.; Chen, J.; Zhang, J.; Chang, J.; Gong, C.; Zhao, Q. Sedimentary evolution of the foreland basin in the NE Tibetan Plateau and the growth of the Qilian Shan since 7 Ma. *GSA Bull.* **2019**, *131*, 1744–1760. [CrossRef]
55. Ma, Z.; Li, X.; Peng, T.; Zhang, J.; Dou, L.; Yu, H.; Liu, J.; Ye, X.; Feng, Z.; Li, M.; et al. Landscape evolution of the Dabanshan planation surface: Implications for the uplift of the eastern tip of the Qilian Mountains since the Late Miocene. *Geomorphology* **2020**, *356*, 107091. [CrossRef]
56. Jolivet, M.; Dominguez, S.; Charreau, J.; Chen, Y.; Li, Y.; Wang, Q. Mesozoic and Cenozoic tectonic history of the central Chinese Tian Shan: Reactivated tectonic structures and active deformation. *Tectonics* **2010**, *29*, TC6019. [CrossRef]
57. De Pelsmaeker, E.; Jolivet, M.; Laborde, A.; Poujol, M.; Robin, C.; Zhimulev, F.I.; Nachtergaele, S.; Glorie, S.; De Clercq, S.; Batalev, V.Y.; et al. Source-to-sink dynamics in the Kyrgyz Tien Shan from the Jurassic to the Paleogene: Insights from sedimentological and detrital zircon U-Pb analyses. *Gondwana Res.* **2018**, *54*, 180–204. [CrossRef]
58. Urueña-Suárez, C.L.; Peñ-Urueñ, M.L.; Muñz-Rocha, J.A.; Rayo-Rocha, L.P.; Villa-mizar-Escalante, N.; Amaya-Ferreira, S.; Ibanez-Mejia, M.; Bernet, M. Zircon U-Pb and fission-track dating applied to resolving sediment provenance in modern rivers draining the Eastern and Central Cordilleras, Colombia. *Geol. Colomb. Vol. 3 Paleogene-Neogene. Serv. Geológico Colomb. Publ. Geológicas Espec.* **2020**, *37*, 1–23.
59. Chen, L.; Wang, Y.; He, P.; Song, C.; Meng, Q.; Feng, W.; Chen, W.; Wang, X. Mesozoic-Cenozoic multistage tectonic deformation of the Qilian Shan constrained by detrital apatite fission track and zircon U-Pb geochronology in the Yumu Shan area. *Tectonophysics* **2021**, *822*, 229151. [CrossRef]
60. Garver, J.I.; Brandon, M.T.; Roden, T.M.; Kamp, P.J. Exhumation history of orogenic highlands determined by detrital fission-track thermochronology. *Geol. Soc. Lond. Spec. Publ.* **1999**, *154*, 283–304. [CrossRef]
61. Carter, A.; Bristow, C.S. Linking hinterland evolution and continental basin sedimentation by using detrital zircon thermochronology: A study of the Khorat Plateau Basin, eastern Thailand. *Basin Res.* **2003**, *15*, 271–285. [CrossRef]
62. Bernet, M.; Garver, J.I. Fission-track Analysis of Detrital Zircon. *Rev. Miner. Geochem.* **2005**, *58*, 205–237. [CrossRef]
63. Carrapa, B.; Bin Hassim, M.F.; Kapp, P.A.; DeCelles, P.G.; Gehrels, G. Tectonic and erosional history of southern Tibet recorded by detrital chronological signatures along the Yarlung River drainage. *GSA Bull.* **2016**, *129*, 570–581. [CrossRef]
64. Dunn, C.A.; Enkelmann, E.; Ridgway, K.D.; Allen, W.K. Source to sink evaluation of sediment routing in the Gulf of Alaska and Southeast Alaska: A thermochronometric perspective. *J. Geophys. Res. Earth Surf.* **2017**, *122*, 711–734. [CrossRef]
65. Glotzbach, C.; Busschers, F.S.; Winsemann, J. Detrital thermochronology of Rhine, Elbe and Meuse river sediment (Central Europe): Implications for provenance, erosion and mineral fertility. *Geol. Rundsch.* **2017**, *107*, 459–479. [CrossRef]
66. Bootes, N.; Enkelmann, E.; Lease, R. Late Miocene to Pleistocene Source to Sink Record of Exhumation and Sediment Routing in the Gulf of Alaska From Detrital Zircon Fission-Track and U-Pb Double Dating. *Tectonics* **2019**, *38*, 2703–2726. [CrossRef]
67. Huyghe, P.; Bernet, M.; Galy, A.; Naylor, M.; Cruz, J.; Gyawali, B.; Gemignani, L.; Mugnier, J.-L. Rapid exhumation since at least 13 Ma in the Himalaya recorded by detrital apatite fission-track dating of Bengal fan (IODP Expedition 354) and modern Himalayan river sediments. *Earth Planet. Sci. Lett.* **2020**, *534*, 116078. [CrossRef]
68. Yamada, R.; Tagami, T.; Nishimura, S.; Ito, H. Annealing kinetics of fission tracks in zircon: An experimental study. *Chem. Geol.* **1995**, *122*, 249–258. [CrossRef]
69. Tagami, T.; Shimada, C. Natural long-term annealing of the zircon fission track system around a granitic pluton. *J. Geophys. Res. Earth Surf.* **1996**, *101*, 8245–8255. [CrossRef]
70. Tian, Y.; Kohn, B.P.; Hu, S.; Gleadow, A.J.W. Postorogenic rigid behavior of the eastern Songpan-Ganze terrane: Insights from low-temperature thermochronology and implications for intracontinental deformation in central Asia. *Geochem. Geophys. Geosyst.* **2013**, *15*, 453–474. [CrossRef]
71. Liu-Zeng, J.; Zhang, J.; McPhillips, D.; Reiners, P.; Wang, W.; Pik, R.; Zeng, L.; Hoke, G.; Xie, K.; Xiao, P.; et al. Multiple episodes of fast exhumation since Cretaceous in southeast Tibet, revealed by low-temperature thermochronology. *Earth Planet. Sci. Lett.* **2018**, *490*, 62–76. [CrossRef]
72. Cheng, F.; Jolivet, M.; Dupont-Nivet, G.; Wang, L.; Yu, X.; Guo, Z. Lateral extrusion along the Altyn Tagh Fault, Qilian Shan (NE Tibet): Insight from a 3D crustal budget. *Terra Nova* **2015**, *27*, 416–425. [CrossRef]
73. Zhao, G.; Wang, Y.; Huang, B.; Dong, Y.; Li, S.; Zhang, G.; Yu, S. Geological reconstructions of the East Asian blocks: From the breakup of Rodinia to the assembly of Pangea. *Earth-Sci. Rev.* **2018**, *186*, 262–286. [CrossRef]
74. Dong, Y.; Sun, S.; Santosh, M.; Zhao, J.; Sun, J.; He, D.; Shi, X.; Hui, B.; Cheng, C.; Zhang, G. Central China Orogenic Belt and amalgamation of East Asian continents. *Gondwana Res.* **2021**, *100*, 131–194. [CrossRef]
75. Wu, C.; Yin, A.; Zuza, A.; Zhang, J.; Liu, W.; Ding, L. Pre-Cenozoic geologic history of the central and northern Tibetan Plateau and the role of Wilson cycles in constructing the Tethyan orogenic system. *Lithosphere* **2016**, *8*, 254–292. [CrossRef]
76. Yin, A.; Nie, S. A Phanerozoic palinspastic reconstruction of China and its neighboring region. In *The Tectonic Evolution of Asia*; Yin, A., Harrison, T.M., Eds.; Cambridge University: New York, NY, USA, 1996; pp. 442–485.
77. Gehrels, G.E.; Yin, A.; Wang, X.-F. Detrital-zircon geochronology of the northeastern Tibetan plateau. *GSA Bull.* **2003**, *115*, 881–896. [CrossRef]
78. Blakey, R.C.; Fielding, C.R.; Frank, T.D.; Isbell, J.L. *Gondwana Paleogeography from Assembly to Breakup—A 500 m. y. Odyssey*; Geological Society of America: Boulder, CO, USA, 2008; Volume 441, pp. 1–28. [CrossRef]
79. Dewey, J.F.; Shackleton, R.M.; Chengfa, C.; Yiyin, S. The tectonic evolution of the Tibetan Plateau. *Philos. Trans. R. Soc. London. Ser. A Math. Phys. Sci.* **1988**, *327*, 379–413.

80. Kapp, P.A.; Yin, A.; Manning, C.; Harrison, T.M.; Taylor, M.; Ding, L. Tectonic evolution of the early Mesozoic blueschist-bearing Qiangtang metamorphic belt, central Tibet. *Tectonics* **2003**, *22*, 1–17. [CrossRef]
81. Jolivet, M. Mesozoic tectonic and topographic evolution of Central Asia and Tibet: A preliminary synthesis. *Geol. Soc. Lond. Spéc. Publ.* **2015**, *427*, 19–55. [CrossRef]
82. Ritts, B.D.; Biffi, U. *Mesozoic Northeast Qaidam Basin: Response to Contractional Reactivation of the Qilian Shan, and Implications for the Extent of Mesozoic Intracontinental Deformation in Central Asia*; Geological Society of America: Boulder, CO, USA, 2001. [CrossRef]
83. Kapp, P.; DeCelles, P.G.; Gehrels, G.E.; Heizler, M.; Ding, L. Geological records of the Lhasa-Qiangtang and Indo-Asian collisions in the Nima area of central Tibet. *GSA Bull.* **2007**, *119*, 917–933. [CrossRef]
84. Chen, S.; Wang, H.; Wei, J.; Lv, Z.; Gan, H.; Jin, S. Sedimentation of the Lower Cretaceous Xiagou Formation and its response to regional tectonics in the Qingxi Sag, Jiuquan Basin, NW China. *Cretac. Res.* **2013**, *47*, 72–86. [CrossRef]
85. Zhang, H.H.; Zhang, Z.C.; Li, J.F. Meso-Cenozoic tectonic evolution in the northeastern margin of the Tibetan Plateau: Evidence from apatite and zircon fission tracks. *Chin. J. Geophys.* **2021**, *64*, 2017–2034. (In Chinese)
86. Wang, Y.; Chen, X.; Zhang, Y.; Yin, Z.; Zuza, A.V.; Yin, A.; Shao, Z. Superposition of Cretaceous and Cenozoic deformation in northern Tibet: A far-field response to the tectonic evolution of the Tethyan orogenic system. *GSA Bull.* **2022**, *134*, 501–525. [CrossRef]
87. Fang, X.; Zhao, Z.; Li, J.; Yan, M.D.; Pan, B.T.; Song, C.H.; Dai, S. Magnetostratigraphy of the late Cenozoic Laojunmiao anticline in the northern Qilian Mountains and its implications for the northern Tibetan Plateau uplift. *China Sci. Earth Sci.* **2005**, *48*, 97–106. [CrossRef]
88. Gansu BGMR (Bureau of Geology and Mineral Resources). *Regional Geology Evolution of Gansu Province*; Geological Publishing House: Beijing, China, 1989; pp. 1–692. (In Chinese)
89. Qinghai BGMR (Bureau of Geology and Mineral Resources). *Regional Geology of Qinghai Province*; Geological Publishing House: Beijing, China, 1991; pp. 1–662. (In Chinese)
90. Gong, H.; Zhao, H.; Xie, W.; Kang, W.; Zhang, R.; Yang, L.; Zhang, Y.; Song, J.; Zhang, Y. Tectono-thermal events of the North Qilian Orogenic Belt, NW China: Constraints from detrital zircon U-Pb ages of Heihe River sediments. *J. Southeast Asian Earth Sci.* **2017**, *138*, 647–656. [CrossRef]
91. Cawood, P.A.; Nemchin, A.A.; Freeman, M.; Sircombe, K. Linking source and sedimentary basin: Detrital zircon record of sediment flux along a modern river system and implications for provenance studies. *Earth Planet. Sci. Lett.* **2003**, *210*, 259–268. [CrossRef]
92. Wang, W.; Zhang, P.; Yu, J.; Wang, Y.; Zheng, D.; Zheng, W.; Zhang, H.; Pang, J. Constraints on mountain building in the northeastern Tibet: Detrital zircon records from synorogenic deposits in the Yumen Basin. *Sci. Rep.* **2016**, *6*, 27604. [CrossRef]
93. Kang, H.; Chen, Y.; Li, D.; Bao, C.; Chen, Y.; Xue, H. Detrital zircon record of rivers' sediments in the North Qilian Orogenic Belt: Implications of the tectonic evolution of the northeastern Tibetan Plateau. *Geol. J.* **2018**, *54*, 2208–2228. [CrossRef]
94. Naeser, N.D.; Zeitler, P.K.; Naeser, C.W.; Cerveny, P.F. Provenance studies by fission-track dating of zircon-etching and counting procedures. *Int. J. Radiat. Appl. Instrum. Part D Nucl. Tracks Radiat. Meas.* **1987**, *13*, 121–126. [CrossRef]
95. Garver, J.I. Etching zircon age standards for fission-track analysis. *Radiat. Meas.* **2003**, *37*, 47–53. [CrossRef]
96. Bernet, M.; Brandon, M.T.; Garver, J.I.; Molitor, B.R. Fundamentals of detrital zircon fission-track analysis for provenance and exhumation studies with examples from the European Alps. *Geol. Soc. Am. Spec. Publ.* **2004**, *378*, 25–36. [CrossRef]
97. Gleadow, A.; Hurford, A.; Quaife, R. Fission track dating of zircon: Improved etching techniques. *Earth Planet. Sci. Lett.* **1976**, *33*, 273–276. [CrossRef]
98. Lanphere, M.A.; Baadsgaard, H. Precise K–Ar, 40Ar/39Ar, Rb–Sr and U/Pb mineral ages from the 27.5 Ma Fish Canyon Tuff reference standard. *Chem. Geol.* **2001**, *175*, 653–671. [CrossRef]
99. Soares, C.J.; Guedes, S.; Hadler, J.C.; Mertz-Kraus, R.; Zack, T.; Iunes, P.J. Novel calibration for LA-ICP-MS-based fission-track thermochronology. *Phys. Chem. Miner.* **2013**, *41*, 65–73. [CrossRef]
100. Donelick, R.A.; O'Sullivan, P.B.; Ketcham, R.A. Apatite Fission-Track Analysis. *Rev. Mineral. Geochem.* **2005**, *58*, 49–94. [CrossRef]
101. Hurford, A.J.; Green, P.F. The zeta age calibration of fission-track dating. *Chem. Geol.* **1983**, *41*, 285–317. [CrossRef]
102. Hasebe, N.; Barbarand, J.; Jarvis, K.; Carter, A.; Hurford, A.J. Apatite fission-track chronometry using laser ablation ICP-MS. *Chem. Geol.* **2004**, *207*, 135–145. [CrossRef]
103. Bernet, M.; van der Beek, P.; Pik, R.; Huyghe, P.; Mugnier, J.-L.; Labrin, E.; Szulc, A. Miocene to Recent exhumation of the central Himalaya determined from combined detrital zircon fission-track and U/Pb analysis of Siwalik sediments, western Nepal. *Basin Res.* **2006**, *18*, 393–412. [CrossRef]
104. Vermeesch, P. On the visualisation of detrital age distributions. *Chem. Geol.* **2012**, *312-313*, 190–194. [CrossRef]
105. Tung, K.-A.; Yang, H.-Y.; Liu, D.-Y.; Zhang, J.-X.; Yang, H.-J.; Shau, Y.-H.; Tseng, C.-Y. The amphibolite-facies metamorphosed mafic rocks from the Maxianshan area, Qilian block, NW China: A record of early Neoproterozoic arc magmatism. *J. Southeast Asian Earth Sci.* **2012**, *46*, 177–189. [CrossRef]
106. Song, S.; Niu, Y.; Su, L.; Zhang, C.; Zhang, L. Continental orogenesis from ocean subduction, continent collision/subduction, to orogen collapse, and orogen recycling: The example of the North Qaidam UHPM belt, NW China. *Earth-Sci. Rev.* **2014**, *129*, 59–84. [CrossRef]

107. Wu, C.; Zuza, A.; Yin, A.; Liu, C.; Reith, R.C.; Zhang, J.; Liu, W.; Zhou, Z. Geochronology and geochemistry of Neoproterozoic granitoids in the central Qilian Shan of northern Tibet: Reconstructing the amalgamation processes and tectonic history of Asia. *Lithosphere* **2017**, *9*, 609–636. [CrossRef]
108. Kang, H.; Chen, Y.-L.; Li, D.-P.; Bao, C.; Zhang, H.-Z. Zircon U-Pb ages and Hf isotopic compositions of fluvial sediments from the Huangshui, Beichuan, and Xichuan rivers, Northwest China: Constraints on the formation and evolution history of the Central Qilian Block. *Geochem. J.* **2018**, *52*, 37–57. [CrossRef]
109. Geng, Y.S.; Zhou, X.W. Early Neoproterozoic granite events in Alax area of Inner Mongolia and their geological significance: Evidence from geochronology. *Acta Petrol. Mineral.* **2010**, *29*, 779–795.
110. Dan, W.; Li, X.-H.; Wang, Q.; Wang, X.-C.; Liu, Y. Neoproterozoic S-type granites in the Alxa Block, westernmost North China and tectonic implications: In situ zircon U-Pb-Hf-O isotopic and geochemical constraints. *Am. J. Sci.* **2014**, *314*, 110–153. [CrossRef]
111. Ge, R.; Zhu, W.; Wilde, S.A.; He, J.; Cui, X.; Wang, X.; Bihai, Z. Neoproterozoic to Paleozoic long-lived accretionary orogeny in the northern Tarim Craton. *Tectonics* **2014**, *33*, 302–329. [CrossRef]
112. Zong, K.; Klemd, R.; Yuan, Y.; He, Z.; Guo, J.; Shi, X.; Liu, Y.; Hu, Z.; Zhang, Z. The assembly of Rodinia: The correlation of early Neoproterozoic (ca. 900 Ma) high-grade metamorphism and continental arc formation in the southern Beishan Orogen, southern Central Asian Orogenic Belt (CAOB). *Precambrian Res.* **2017**, *290*, 32–48. [CrossRef]
113. Li, Z.X.; Li, X.H.; Kinny, P.D.; Wang, J.; Zhang, S.; Zhou, H. Geochronology of Neoproterozoic syn-rift magmatism in the Yangtze Craton, South China and correlations with other continents: Evidence for a mantle superplume that broke up Rodinia. *Precambrian Res.* **2003**, *122*, 85–109. [CrossRef]
114. Charvet, J. The Neoproterozoic–Early Paleozoic tectonic evolution of the South China Block: An overview. *J. Southeast Asian Earth Sci.* **2013**, *74*, 198–209. [CrossRef]
115. Li, S.; Li, X.; Wang, G.; Liu, Y.; Wang, Z.; Wang, T.; Cao, X.; Guo, X.; Somerville, I.; Li, Y.; et al. Global Meso-Neoproterozoic plate reconstruction and formation mechanism for Precambrian basins: Constraints from three cratons in China. *Earth-Sci. Rev.* **2019**, *198*, 102946. [CrossRef]
116. Roger, F.; Jolivet, M.; Malavieille, J. The tectonic evolution of the Songpan-Garzê (North Tibet) and adjacent areas from Proterozoic to Present: A synthesis. *J. Southeast Asian Earth Sci.* **2010**, *39*, 254–269. [CrossRef]
117. Li, M.; Wang, C.; Li, R.; Meert, J.G.; Peng, Y.; Zhang, J. Identifying late Neoproterozoic-early Paleozoic sediments in the South Qilian Belt, China: A peri-Gondwana connection in the northern Tibetan Plateau. *Gondwana Res.* **2019**, *76*, 173–184. [CrossRef]
118. Meert, J.G.; Torsvik, T.H. The making and unmaking of a supercontinent: Rodinia revisited. *Tectonophysics* **2003**, *375*, 261–288. [CrossRef]
119. Xu, B.; Jian, P.; Zheng, H.; Zou, H.; Zhang, L.; Liu, D. U–Pb zircon geochronology and geochemistry of Neoproterozoic volcanic rocks in the Tarim Block of northwest China: Implications for the breakup of Rodinia supercontinent and Neoproterozoic glaciations. *Precambrian Res.* **2005**, *136*, 107–123. [CrossRef]
120. Fu, D.; Kusky, T.; Wilde, S.A.; Polat, A.; Huang, B.; Zhou, Z. Early Paleozoic collision-related magmatism in the eastern North Qilian orogen, northern Tibet: A linkage between accretionary and collisional orogenesis. *GSA Bull.* **2018**, *131*, 1031–1056. [CrossRef]
121. Xu, Y.; Du, Y.; Cawood, P.A.; Yang, J. Provenance record of a foreland basin: Detrital zircon U–Pb ages from Devonian strata in the North Qilian Orogenic Belt, China. *Tectonophysics* **2010**, *495*, 337–347. [CrossRef]
122. Song, D.; Glorie, S.; Xiao, W.; Collins, A.S.; Gillespie, J.; Jepson, G.; Li, Y. Tectono-thermal evolution of the southwestern Alxa Tectonic Belt, NW China: Constrained by apatite U-Pb and fission track thermochronology. *Tectonophysics* **2018**, *722*, 577–594. [CrossRef]
123. Zhang, J.; Wang, Y.; Qu, J.; Zhang, B.; Zhao, H.; Yun, L.; Li, T.; Niu, P.; Nie, F.; Hui, J.; et al. Mesozoic intracontinental deformation of the Alxa Block in the middle part of Central Asian Orogenic Belt: A review. *Int. Geol. Rev.* **2021**, *63*, 1490–1520. [CrossRef]
124. Roger, F.; Arnaud, N.; Gilder, S.; Tapponnier, P.; Jolivet, M.; Brunel, M.; Malavieille, J.; Xu, Z.; Yang, J. Geochronological and geochemical constraints on Mesozoic suturing in east central Tibet. *Tectonics* **2003**, *22*, 1037. [CrossRef]
125. Roger, F.; Jolivet, M.; Malavieille, J. Tectonic evolution of the Triassic fold belts of Tibet. *Comptes Rendus Geosci.* **2008**, *340*, 180–189. [CrossRef]
126. Cheng, F.; Jolivet, M.; Hallot, E.; Zhang, D.; Zhang, C.; Guo, Z. Tectono-magmatic rejuvenation of the Qaidam craton, northern Tibet. *Gondwana Res.* **2017**, *49*, 248–263. [CrossRef]
127. Zhang, B.; Zhang, J.; Wang, Y.; Zhao, H.; Li, Y. Late Mesozoic-Cenozoic Exhumation of the Northern Hexi Corridor: Constrained by Apatite Fission Track Ages of the Longshoushan. *Acta Geol. Sin.-Engl. Ed.* **2017**, *91*, 1624–1643. [CrossRef]
128. Liu, D.; Li, H.; Chevalier, M.-L.; Sun, Z.; Pei, J.; Pan, J.; Ge, C.; Wang, P.; Wang, H.; Wu, C. Activity of the Baiganhu Fault of the Altyn Tagh Fault System, northern Tibetan Plateau: Insights from zircon and apatite fission track analyses. *Palaeogeogr. Palaeoclim. Palaeoecol.* **2021**, *570*, 110356. [CrossRef]
129. Shi, G.; Soares, C.J.; Shen, C.; Wang, H.; Yang, C.; Liang, C.; Liu, M. Combined detrital zircon fission track and U-Pb dating of the Late Paleozoic to Early Mesozoic sandstones in the Helanshan, western Ordos fold-thrust belt: Constraints for provenance and exhumation history. *J. Geodyn.* **2019**, *130*, 57–71. [CrossRef]
130. Peng, H.; Wang, J.; Liu, C.; Zhang, S.; Zattin, M.; Wu, N.; Feng, Q. Thermochronological constraints on the Meso-Cenozoic tectonic evolution of the Haiyuan-Liupanshan region, northeastern Tibetan Plateau. *J. Southeast Asian Earth Sci.* **2019**, *183*, 103966. [CrossRef]

131. Peng, N.; Liu, Q.; Kuang, W.; Chen, J.; Xue, P.L.; Xu, J.L.; Liu, H.; Liu, Y.X.; Xu, H.; Dong, C. The provenance of Lower Cretaceous basin in the Qilian Mountain-Beishan area: Evidence from paleocurrents, gravels, sandstone compositions and detrital zircon geochronology. *Geol. Bull. China* **2013**, *32*, 456–475. (In Chinese)
132. Cheng, F.; Garzione, C.; Jolivet, M.; Wang, W.; Dong, J.; Richter, F.; Guo, Z. Provenance analysis of the Yumen Basin and northern Qilian Shan: Implications for the pre-collisional paleogeography in the NE Tibetan plateau and eastern termination of Altyn Tagh fault. *Gondwana Res.* **2018**, *65*, 156–171. [CrossRef]
133. Zhao, Z.-B.; Li, C.; Ma, X.-X. How does the elevation changing response to crustal thickening process in the central Tibetan Plateau since 120 Ma? *China Geol.* **2021**, *4*, 32–43. [CrossRef]
134. Cogné, J.-P.; Kravchinsky, V.A.; Halim, N.; Hankard, F. Late Jurassic-Early Cretaceous closure of the Mongol-Okhotsk Ocean demonstrated by new Mesozoic palaeomagnetic results from the Trans-Baïkal area (SE Siberia). *Geophys. J. Int.* **2005**, *163*, 813–832. [CrossRef]
135. Jolivet, M.; De Boisgrollier, T.; Petit, C.; Fournier, M.; Sankov, V.A.; Ringenbach, J.-C.; Byzov, L.; Miroshnichenko, A.I.; Kovalenko, S.N.; Anisimova, S.V. How old is the Baikal Rift Zone? Insight from apatite fission track thermochronology. *Tectonics* **2009**, *28*, TC3008. [CrossRef]
136. Van der Voo, R.; van Hinsbergen, D.J.; Domeier, M.; Spakman, W.; Torsvik, T.H. *Latest Jurassic–Earliest Cretaceous Closure of the Mongol-Okhotsk Ocean: A Paleomagnetic and Seismological-Tomographic Analysis*; Geological Society of America: Boulder, CO, USA, 2015; Volume 513, pp. 589–606. [CrossRef]
137. Qi, B.; Hu, D.; Yang, X.; Zhang, Y.; Tan, C.; Zhang, P.; Feng, C. Apatite fission track evidence for the Cretaceous–Cenozoic cooling history of the Qilian Shan (NW China) and for stepwise northeastward growth of the northeastern Tibetan Plateau since early Eocene. *J. Southeast Asian Earth Sci.* **2016**, *124*, 28–41. [CrossRef]
138. Wu, C.; Zuza, A.V.; Li, J.; Haproff, P.J.; Yin, A.; Chen, X.; Ding, L.; Li, B. Late Mesozoic–Cenozoic cooling history of the northeastern Tibetan Plateau and its foreland derived from low-temperature thermochronology. *GSA Bull.* **2021**, *133*, 2393–2417. [CrossRef]
139. Yin, A.; Dang, Y.-Q.; Wang, L.-C.; Jiang, W.-M.; Zhou, S.-P.; Chen, X.; Gehrels, G.E.; McRivette, M.W. Cenozoic tectonic evolution of Qaidam basin and its surrounding regions (Part 1): The southern Qilian Shan-Nan Shan thrust belt and northern Qaidam basin. *GSA Bull.* **2008**, *120*, 813–846. [CrossRef]
140. Li, Q.; Pan, B.; Hu, X.; Hu, Z.; Li, F.; Yang, S. Apatite fission track constraints on the pattern of faulting in the north Qilian Mountain. *J. Earth Sci.* **2013**, *24*, 569–578. [CrossRef]
141. Jian, X.; Guan, P.; Zhang, W.; Liang, H.; Feng, F.; Fu, L. Late Cretaceous to early Eocene deformation in the northern Tibetan Plateau: Detrital apatite fission track evidence from northern Qaidam basin. *Gondwana Res.* **2018**, *60*, 94–104. [CrossRef]
142. Wang, X.; Song, C.; Zattin, M.; He, P.; Song, A.; Li, J.; Wang, Q. Cenozoic pulsed deformation history of northeastern Tibetan Plateau reconstructed from fission-track thermochronology. *Tectonophysics* **2016**, *672-673*, 212–227. [CrossRef]
143. Wang, F.; Shi, W.; Zhang, W.; Wu, L.; Yang, L.; Wang, Y.; Zhu, R. Differential growth of the northern Tibetan margin: Evidence for oblique stepwise rise of the Tibetan Plateau. *Sci. Rep.* **2017**, *7*, srep41164. [CrossRef]
144. Wu, C.; Li, J.; Zuza, A.V.; Liu, C.; Liu, W.; Chen, X.; Jiang, T.; Li, B. Cenozoic cooling history and fluvial terrace development of the western domain of the Eastern Kunlun Range, northern Tibet. *Palaeogeogr. Palaeoclim. Palaeoecol.* **2020**, *560*, 109971. [CrossRef]
145. Zattin, M.; Wang, X. Exhumation of the western Qinling mountain range and the building of the northeastern margin of the Tibetan Plateau. *J. Asian Earth Sci.* **2019**, *177*, 307–313. [CrossRef]